Bridging Photosynthesis and Crop Yield Formation with a Mechanistic Model of Whole Plant Carbon Nitrogen Interaction

Tian-Gen Chang and Xin-Guang Zhu*

Key Laboratory for Plant Molecular Genetics, Center of Excellence for Molecular Plant Sciences, Chinese Academy of Sciences, Shanghai 200032, China

*Correspondence: zhuxg@cemps.ac.cn

ABSTRACT

Crop yield is co-determined by photosynthetic potential of source organs, and pattern of partitioning and utilization of photosynthate among sink organs. Although correlation between source sink relation and grain yield has been studied for a century, a quantitative understanding of the metabolic basis of source sink interaction is lacking. Here, we describe a mechanistic model of Whole plAnt Carbon Nitrogen Interaction (WACNI), enabling precise prediction of plant physiological dynamics during the grain filling period by reconstructing primary metabolic and biophysical processes in source, sink and transport organs. To get a specified range of parameters required to quantify the enzymatic kinetics in rice, a data set is established based on case studies and natural variation surveys in the past decades. The parameterized model quantitatively predicts plant carbon and nitrogen budget upon various scenarios, ranging from field management and environmental perturbation to genetic manipulation, thus enabling dissection of the precise role of such alterations in crop yield formation. Model simulations further reveal the importance of re-allocating activity of carbon/nitrogen metabolic and transport processes for a plant physiological ideotype to maximize crop yield.

Key words: carbon nitrogen metabolism, crop yield, grain filling, ideotype, photosynthesis, plant physiology, source sink interaction, systems model

INTRODUCTION

As the global climate changes, population increases, arable land decreases, there is a tremendous need for the next green revolution to greatly increase the crop yield once again [1-4]. With the available identification of a large number of molecular markers controlling important traits in plants, molecular breeding by rational design, is becoming a new route for crop improvement [5-9]. In addition to the advances in functional genomics research, other major drivers of this crop improvement route include advances in phenomics technology and genome editing technology [10-13]. To date, one key remaining issue is the quantification of crop ideotype as an objective during crop genetic engineering [14].

Crop ideotype includes both morphological and physiological characteristics, which together determine canopy photosynthesis and whole-plant source sink relation, thus define the crop yield potential [15-18]. Ever since the proposal of the wheat ideotype by Donald [19], improving crop morphology has been extensively studied in genetic research, modeling research, and in crop high-yield breeding, which is largely responsible for the dramatic increase in rice grain yield from around 3 t ha^{-1} to up to 15 t ha^{-1} in the past 60 years [17,20-26]. Although long recognized as the other equally important factor of crop ideotype [27-29], crop physiological parameters, i.e., characteristics associated with photosynthesis, respiration, carbon and nitrogen

metabolism in different organs, and also the transport of metabolites between organs, have so far generated little impact in crop breeding. This is due to there is still no consensus on the optimal physiological characteristics associated with a crop ideotype. In the past century, results from individual field experiments often contradicted with each other, due to different weather and soil conditions of the experimental sites, and/or the use of different crops or cultivars or management practices [30].

Systems modeling approach is recognized as a promising means to guide design of the optimal crop physiological characteristics to achieve high yield [30-33]. As a result of research by plant systems modeling community during the past decades, mechanistic models for a number of individual plant physiological processes, such as leaf photosynthesis [34,35], phloem long-distance carbon transport transport [36], flowering time determination [37,38] and root growth and development [39], have been developed. These mechanistic models have been used to guide improvement of photosynthesis for greater efficiency [2,40-43] and evaluate the impact of modifying photosynthesis for crop yields [44]. Missing in the current repertoire of models is a mechanistic framework model connecting metabolism within individual source/sink organs and transport of metabolites between these organs, where the consequence on plant growth and development is predicted as an emergent property.

Carbon and nitrogen metabolism are the basis for plant growth and development [45]. To predict crop yield formation directly from the molecular processes in different source and sink organs, and the carbon and nitrogen fluxes between organs, we develop a mechanistic model of **W**hole pl**A**nt **C**arbon **N**itrogen **I**nteraction (WACNI). As a fully mechanistic model, WACNI not only enables us to quantify plant carbon and nitrogen budget under different source sink relation alteration scenarios and to define the physiological features associated with crop ideotype, but also serves to design molecular manipulations to approach such an ideotype. Thus, a combination of this theoretical framework and the advanced genome editing technologies [46,47] will offer unprecedented opportunity in engineering crop physiological features for greater yield.

RESULTS

Construction of WACNI: a mechanistic model of plant grain yield formation

WACNI is an ordinary differentiation equations (ODEs) based kinetic model predicting plant-level physiological dynamics from the flowering to the harvest stage. It comprises five modules, i.e., root, leaf, grain, stem (including culm and sheath) and vascular transport system (xylem and phloem). Metabolites exchange between modules by trans-membrane transport (Figure 1). Fourteen types of biochemical and

biophysical processes involved in different source/sink/transport organs are mathematically represented in WACNI (Figure 1). Briefly, these processes include assimilation, transport and utilization of six representative primary metabolites, i.e., triose phosphates (TP), sucrose (Suc), starch, inorganic nitrogen (I-N, including NH_4^+ and NO_3^-), free form of organic nitrogen (O-N, including amino acids and amides), and proteins. Further, WACNI also incorporates the interaction between these metabolites and plant developmental processes, e.g. root growth, grain volume expansion (endosperm cell division), grain filling (starch and protein cumulation in endosperm), root senescence and leaf senescence (Figure 1; see Methods). The apparent kinetic parameters for each process, initial metabolite concentrations and carbon/nitrogen mass in different organs at the flowering stage are input variables for the model.

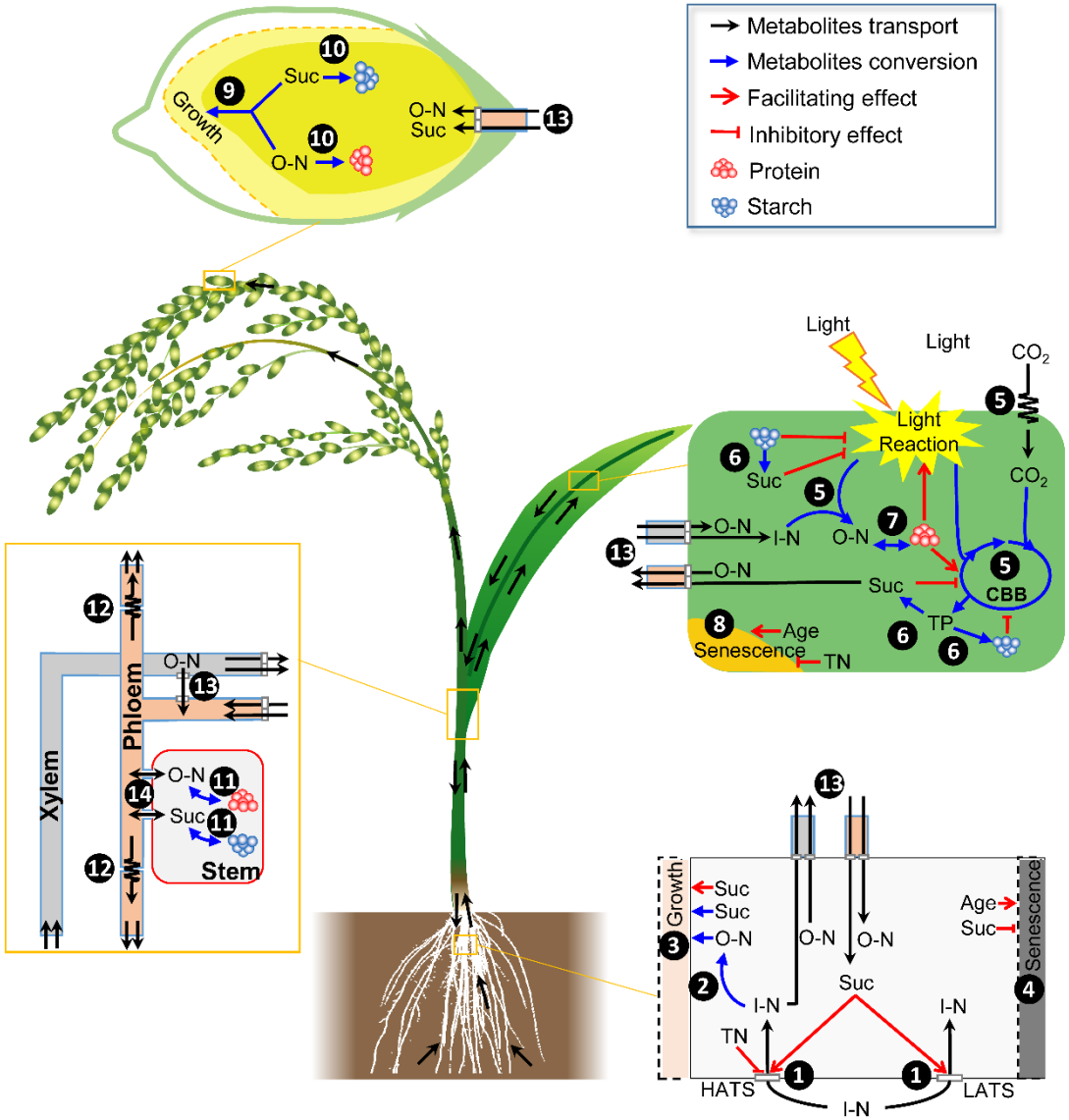

Figure 1. A mechanistic model of plant grain yield formation during rice grain filling period. Abbreviations: Suc, sucrose; TP, triose phosphates; I-N, inorganic nitrogen; O-N, free-form organic nitrogen; TN, total mobile nitrogen, including I-N, O-N and protein; HATS, high-affinity nitrogen transport system; LATS, low-affinity nitrogen transport system; CBB, Calvin–Benson–Bassham cycle. The 14 groups of processes illustrated in the figure are: 1, root nitrogen uptake; 2, root nitrogen assimilation; 3, root growth; 4, root senescence; 5, leaf CO_2 and nitrogen assimilation; 6, leaf triose phosphate, sucrose and starch interconversion; 7, leaf organic nitrogen and protein interconversion; 8, leaf senescence; 9, grain volume growth (cell division); 10, grain starch and protein synthesis; 11, stem sucrose and starch, organic nitrogen and protein interconversion; 12, phloem long distance transport; 13, transporter-dependent short distance transport; 14, symplastic diffusion between phloem and stem.

Parameterization of WACNI: formation of a primary reference dataset on natural variation of important rice traits based on bibliomics

Firstly, we have simplified the representation of each process to reduce the required number of parameters to be estimated (see Methods). Then, for each required parameter, its value or value range was determined based on the available literature in rice. Specifically, for most morphological and agronomic parameters, their natural variations were determined from independent case studies, large-scale surveys on genetic populations or from the reviews. For determining a certain parameter controlling capacity of a certain process, maximal activity of the rate limiting enzyme in this process was used in the first priority; if the maximal activity was not available, the maximal metabolic flux of this process would be used (see details in Supplementary Table 1). Finally, a comprehensive dataset for natural variation of many important parameters determining rice growth and development was generated (Supplementary Table 1).

Physiological dynamics and carbon & nitrogen economy during rice grain filling period

After parameterization, WACNI realistically predicted, during the grain filling period, changes in root weight (Figure 2a, R^2=0.94), leaf area (Figure 2b, R^2=0.96), rates of canopy photosynthesis (Figure 2c, R^2=0.96), grain volume (Figure 2d, R^2=0.99), grain

dry weight (Figure 2e, R^2=1.00) and stem non-structural carbohydrates (Figure 2f, R^2=0.99). In addition, a plant-level carbon and nitrogen budget throughout the whole grain filling period was generated (Figure 2g). For the carbon budget, WACNI predicted that 21.6% and 52.1% of the photosynthetically fixed carbon could be respired by the leaf itself and by the entire plant, respectively, which were close to the previous estimates of 20% and 40-60% in cultivated plants, respectively [48]. WACNI predicted an 88.0% and 12.0% contribution from photosynthesis-derived carbon and pre-flowering non-structural carbohydrate storage in stem to grain filling, respectively. The 'apparent contribution' of pre-flowering stem non-structural carbohydrate storage to grain yield, i.e., the ratio between the stem weight loss during grain filling to the grain yield at the harvest stage, was predicted to be 27.3%, which coincides with the observed value in the range of 0 to 40% [49]. Namely, our simulation demonstrates that the frequently used 'apparent contribution', which omits respiration of the grain and the stem, is a substantial over-estimate of the actual contribution of pre-flowering stem non-structural carbohydrate storage to grain yield (e.g. 27.3% versus 12.0% in our case). In addition, 19.8% of the total carbohydrates was predicted to be partitioned to the root from the flowering stage to the harvest stage, while the remaining 80.2% to the grain.

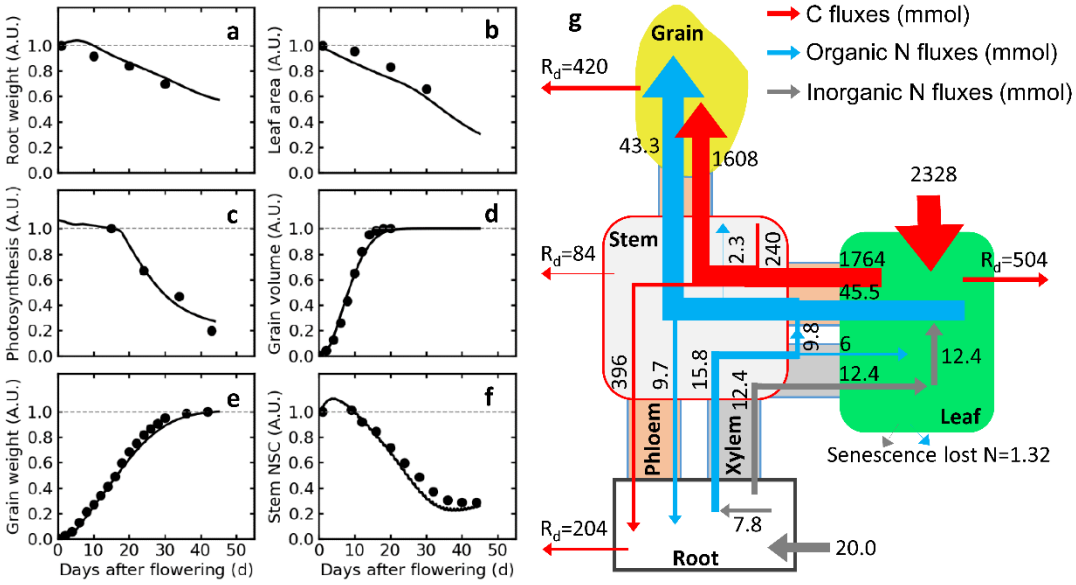

Figure 2. Prediction of plant physiological dynamics (A-F) and carbon & nitrogen economy (G) during rice grain filling period. **a**, root dry weight (R2=0.94; data from [50]); **b**, leaf area (R2=0.96; data from [51]); **c**, diurnal canopy photosynthesis (R2=0.96; data from [52]); **d**, grain volume (R2=0.99; data from [53]); **e**, grain dry weight (R2=1.00; data from [53]); **f**, stem non-structural carbohydrates content (R2=0.99; data from [54]). (A-F), the solid lines are modeled data, the dots are measured data. **g**, carbon and nitrogen fluxes (mmol) within the whole plant throughout the whole grain filling period. Abbreviations: R_d, dark respiration; C fluxes, carbon fluxes; N fluxes, nitrogen fluxes.

For the nitrogen budget, WACNI predicted 38.6% of newly absorbed nitrogen to be assimilated in the root, while 61.4% to be in the leaf. The total plant nitrogen content at the flowering stage was 49 mmol (see Methods); thus, the root nitrogen uptake after flowering accounts for 29.0% of the whole season nitrogen uptake, which is close to the reported value, i.e., 30% [55]. In addition, the nitrogen harvest index, i.e., the ratio between the amount of nitrogen stored in the grain at the harvest stage and the total plant nitrogen uptake during the whole growth season, was 62.8%, which is also in

the known range of 30-77% , based on a large scale survey on irrigated lowland rice in tropical and subtropical Asia [56].

Carbon and nitrogen dynamics in leaves and grains during grain filling can be reproduced in silico without re-allocation of enzyme activities across different nitrogen regimes

We then tested the performance of WACNI under different field management practices and environmental perturbations. Firstly, we simulated changes in the leaf nitrogen concentration, the grain nitrogen concentration, and the grain dry weight dynamics during the grain filling period under different nitrogen application rates (Figure 3a-l). WACNI reproduced patterns of leaf nitrogen concentration dynamics from the flowering stage to the harvest stage for all nitrogen treatment groups (Figure 3a, R^2=0.97; Figure 3d, R^2=0.92; Figure 3g, R^2=0.97; Figure 3j, R^2=0.94), except for an over-estimate of the leaf nitrogen concentration beyond 28 days after flowering for the low nitrogen and medium nitrogen groups (Figure 3d, g). Remarkably, WACNI not only precisely predicted the relative values of grain nitrogen concentration and grain yield at the harvest stage, but also reproduced the dynamic changes of grain nitrogen concentration (Figure 3b, R^2=0.97; Figure 3e, R^2=0.97; Figure 3h, R^2=0.98; Figure 3k, R^2=0.95) and the pattern of grain dry weight gain (Figure 3c, R^2=0.94; Figure 3f, R^2=0.98; Figure 3i, R^2=1.00; Figure 3l, R^2=0.96) throughout the grain

filling period for all treatments, without re-allocating activity of metabolic and transport processes across different nitrogen regimes.

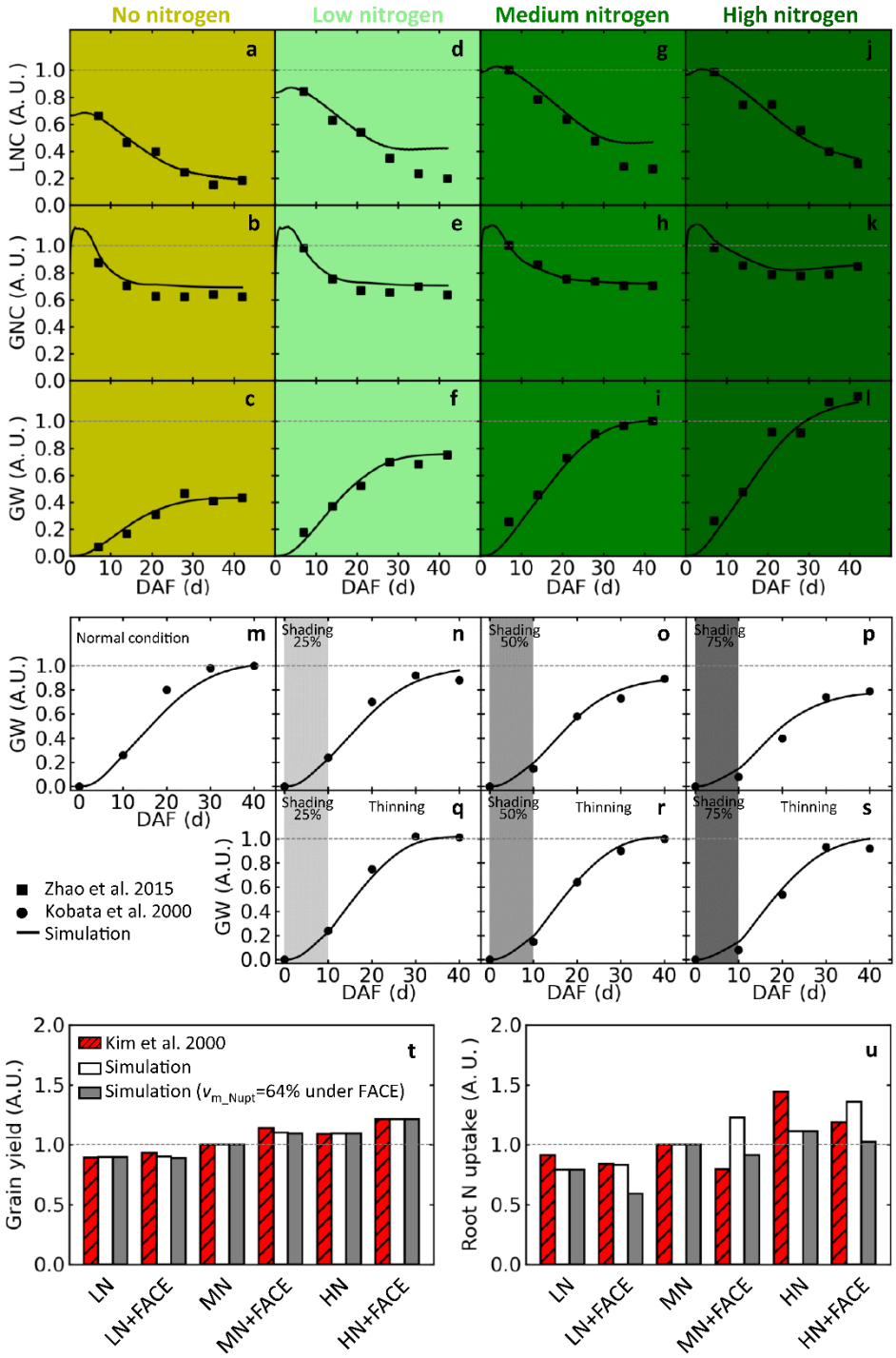

Figure 3. Predicted relative changes of plant physiological status and agronomic traits under different nitrogen application rates (a-l), light regimes (m-s), and air CO_2 concentrations (t-u). Dynamic changes of leaf nitrogen concentration, grain nitrogen

concentration and grain dry weight with no nitrogen (**a**, R^2=0.97**; b**, R^2=0.97**; c**, R^2=0.94), low level nitrogen (**d**, R^2=0.92**; e**, R^2=0.97**; f**, R^2=0.98), medium level nitrogen (**g**, R^2=0.97**; h**, R^2=0.98**; i**, R^2=1.00) or high level nitrogen (**j**, R^2=0.94**; k**, R^2=0.95**; l**, R^2=0.96) applied during the ear development period. Grain filling pattern under normal condition (**m**, R^2=0.98); shading treatments during the first 10 days after flowering which reduce the solar radiation by 25% (**n**, R^2=0.98), 50% (**o**, R^2=0.99) and 75% (**p**, R^2=0.98); shading treatments followed by spacing (thinning the every other plants to reduce the plant density by half; **q**, R^2=0.99**; r**, R^2=1.00**; s**, R^2=0.99). Grain yield at the harvest stage (**t**) and total root nitrogen uptake during the grain filling period (**u**) for plants grown under ambient CO_2 concentration with low nitrogen ('LN'), medium nitrogen ('MN') and high nitrogen ('HN') application rates, and plants grown under free air CO_2 enrichment (FACE) condition with low nitrogen ('LN+FACE'), medium nitrogen ('MN+FACE') and high nitrogen ('HN+FACE') application rates. (**a-s**), the dots are measured data, the solid lines are modeled data. (**t-u**), the black bars are measured data, the white bars are modeled data, the grey bars are modeled data with additional assumption of the maximal root nitrogen uptake rate under FACE conditions to be 64% of that under ambient conditions. The experimental data are from [57] for panels a-l, from [58] for panels m-s, from [59] for panels t-u. Abbreviations: LNC, leaf nitrogen concentration; GNC, grain nitrogen concentration; GDW, grain dry weight; DAF, days after flowering.

Low light during early grain filling period affects grain weight gain pattern but does NOT compromise rice yield potential

When we simulated grain filling under different light regimes (Figure 3m-s), WACNI predicted an increased penalization to grain dry weight at 10 days after flowering, as well as at the harvest stage when 25%, 50% or 75% of the incident irradiance was shaded during the first 10 days after flowering (Figure 3m, R^2=0.98; Figure 3n, R^2=0.98; Figure 3o, R^2=0.99; Figure 3p, R^2=0.98). In addition, WACNI successfully predicted an acceleration of grain filling rate beyond 10 days after flowering when extra light penetrates into the canopy as a result of plant thinning. Thus, it provides

theoretical support to the idea that short-term impaired grain filling by low light-induced shortage of assimilates can almost be fully compensated if sufficient resource is provided later (Figure 3q, R^2=0.99; Figure 3r, R^2=1.00; Figure 3s, R^2=0.99)[58].

Inhibited root nitrogen uptake capacity during grain filling under elevated air CO_2 concentration underlies reduced plant nitrogen budget

When we simulated grain yield and root nitrogen uptake under different atmospheric CO_2 concentration, and soil nitrogen application rates, WACNI correctly predicted that grain yield increased with nitrogen application rate under both ambient CO_2 level and elevated CO_2 concentration (Figure 3t). Moreover, simulations using WACNI also confirmed the observation that grain yield would benefit more from the elevated CO_2 concentration under medium and high nitrogen application rates (10.8% and 11% enhancement of grain yield, respectively) than that under low nitrogen application rate (1% enhancement of grain yield; Figure 3t). However, when plants with the same nitrogen application rates were compared, WACNI predicted higher total root nitrogen uptake during the grain filling period of plants grown under elevated CO_2 concentration than that of plants grown under ambient CO_2 concentration, which was, however, against the experimental observation (Figure 3u). Earlier, the nitrogen uptake capacity per root dry weight was shown to be unaffected under FACE at the young panicle development period, but reduced by 31-41% from the flowering stage

to the harvest stage compared to the plants grown under ambient CO_2 concentration [60]. Remarkably, if a mean percentage reduction of maximal root nitrogen uptake rate, 36%, was set under elevated air CO_2 concentration in WACNI, both the relative trend of grain yield and root nitrogen uptake during the grain filling period could be reproduced (the 'v_{m_Nupt}=64% under FACE' labeled simulations in Figure 3t, u), which demonstrates the importance of root nitrogen uptake capacity in characterizing plant carbon/nitrogen budget under elevated air CO_2 concentration.

Prolonged leaf functional duration greatly benefits grain yield with a slight reduction in grain nitrogen concentration

We further tested WACNI by predicting the responses of grain yield, plant physiological traits and agronomic traits to genetic manipulations that affect source sink relation. We first simulated the impact on grain yield related traits when the senescence of the major carbon source, leaf, was perturbed. We simulated leaf nitrogen concentration dynamics during the grain filling period, the grain yield and grain nitrogen concentration at the harvest stage for rice plants with different activities of leaf protein degradation. According to Liang, et al. [61], three scenarios could be examined, and we indeed showed: (1) promoted leaf protein degradation activity mimicking the *ps1-D* mutant and *OsNAP* overexpression plants (the '*ps1-D*' and 'OE' groups in Figure 4a-c); (2) medium leaf protein degradation activity mimicking wild

type plants (the 'WT' group in Figure 4a-c); and (3) reduced leaf protein degradation activity mimicking *OsNAP* RNAi plants (the 'RNAi' group in Figure 4b-c). As a result, WACNI predicted a faster leaf nitrogen loss of the *ps1-D* mutant plants, as a result of the accelerated leaf protein degradation rate, which mimicked the observed faster decrease in chlorophyll content in the *ps1-D* mutant (Figure 4a, R^2=0.86 for WT and R^2=0.92 for ps1-D mutant). Concurrently, WACNI also predicted an increase of grain yield at the expense of a slight decrease in grain nitrogen concentration for the 'RNAi' plant and the opposite for the 'OE' group plants, both of which coincided well with experimental observations (Figure 4b, c). The enhanced grain yield was mainly contributed by the increased higher canopy photosynthesis in the later grain filling period as a result of larger leaf area and higher leaf nitrogen concentration, whereas the reduced grain nitrogen concentration was mainly attributed to the decreased nitrogen concentration in the phloem as a result of less leaf nitrogen remobilization (Supplementary Figure 1; Figure 4a).

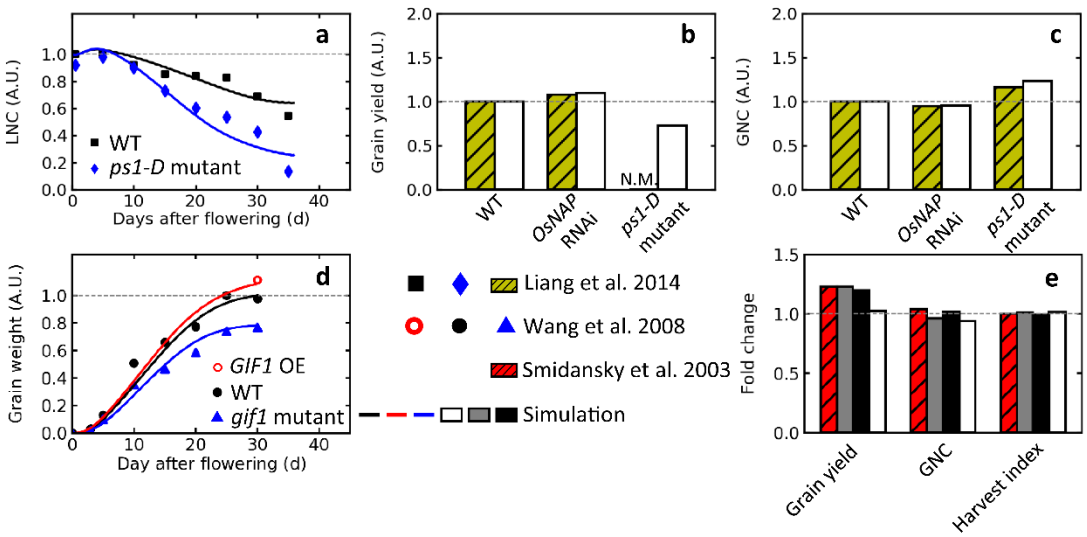

Figure 4. Predicted relative changes of plant physiological status and agronomic traits under different source (a-c), transport (d-i) or sink (j-l) related genetic manipulations. **a**, leaf nitrogen concentration dynamic change during the grain filling period for the wild type (WT; R^2=0.86) and a *OsNAP* gain-of-function mutant, prematurely senile 1 (*ps1-D* mutant; R^2=0.92). Relative grain yield (**b**) and grain nitrogen concentration (**c**) of *ps1-D* mutant and the *OsNAP* RNAi transgenic plant to the WT. **d**, grain dry weight dynamic change of the wild type (WT; R^2=0.98), a cell-wall invertase gene loss-of-function mutant, grain incomplete filling 1 (*gif1* mutant; R^2=0.98), and the *GIF1* over-expression transgenic line (*GIF1* OE). **e**, relative changes of grain yield, grain nitrogen concentration and harvest index for plants expressing a modified maize AGPase large subunit sequence (*Sh2r6hs*) under control of an endosperm-specific promoter. The experimental data are from [61] for panels a-c, from [62] for panel d, from [63] for panel e. Abbreviations: LNC, leaf nitrogen concentration; GNC, grain nitrogen concentration; N.M., not measured.

Sucrose transport capacity is a major factor determining grain filling rate

We then simulated the consequences of perturbing the sucrose transport system. Here we tested the effect of changing capacity of sucrose unloading into the grain on grain filling rate and the final grain yield. Wang, et al. [62] reported that a gene *GIF1*, which encodes a cell-wall invertase, is required for sucrose transport to the grain. In agreement with the experimental results, grain filling rate was predicted to be faster for *GIF1* overexpression plants, which had a higher sucrose unloading capacity. Further, the grain filling rate was predicted to be slower for *gif1* mutant plants which had decreased sucrose unloading capacity (Figure 4d, R^2=0.98 for both WT and *gif1* mutant). Although Wang, et al. [62] had suggested that the *GIF1* gene could increase the yield potential through improved grain-filling, the grain yield of *GIF1* overexpression plants was not shown in their experiments. Here, we simulated two scenarios: (1)

plants with parameter values set according to Wang, et al. [62], which represented a 'sink limited' scenario; (2) plants with default parameter values except that the grain number per ear was set to 190, which represents a 'source limited' scenario. As a result, when plants were 'sink limited', enhancing maximal rate of sucrose unloading to the grain ($v_{m_grain_Suc_ul}$) increased both the grain filling rate and the final grain yield, whereas reducing $v_{m_grain_Suc_ul}$ decreased the grain filling rate , as well as the final grain yield (Supplementary Figure 2). However, when plants were 'source limited', enhancing $v_{m_grain_Suc_ul}$ could increase grain filling rate only in the early phase of grain filling period, whereas the final grain yield even decreased, which was mainly due to faster sink growth induced accelerated leaf nitrogen remobilization and the consequently earlier leaf senescence (Supplementary Figure 3). We note that although larger sugar flow directed towards sinks may relieve 'feedback downregulation' of photosynthesis, for those 'source limited' cultivars, the unloading rate of sucrose to grains should be limited to avoid unusually fast draining of nutrients from the leaves since this causes earlier senescence of the whole plant. Consistent with this notion, overexpression of *PbSWEET4*, a sugar transporter gene in pear, is known to cause early senescence in leaves [64]. Similarly, overexpression of *OsSWEET5* in rice, which encodes a sugar transporter protein in leaves, stem, root and floral organs, causes precocious leaf senescence [65].

Enhanced endosperm ADP-glucose pyrophosphorylase activity is not the mechanism

for rice with ectopic expression of Sh2r6hs to gain increased grain yield

Here, we present our results on simulating the consequences of altering the grain storage capacity. Endosperm-specific ectopic expression of a modified maize ADP-glucose pyrophosphorylase (AGPase) large subunit sequence (*Sh2r6hs*) has been shown to enhance the activity of starch synthesis in the endosperm of both wheat and rice [63,66]. In our work, we simulated the effects of increasing the maximal grain starch synthesis rate ($v_{m_grain_Star_syn}$) to 150% of its default value, on grain yield and yield related traits; this represented an *in silico Sh2r6hs* ectopic expression plant. As a reference, in the actual *Sh2r6hs* transgenic plants, the measured AGPase activity in developing grains was higher (from as small as 9% to as high as 52%) than in wild type plants, 10-20 days after flowering [63]. We note that WACNI realistically predicted the increase of grain yield and the maintenance of harvest index, although it predicted a slight decrease, rather than the observed slight increase, in grain nitrogen concentration for the *Sh2r6hs* transgenic plants at the harvest time (Figure 4e). Further, we note that although *Sh2r6hs* was expressed under the control of an endosperm-specific promoter, the size of transgenic plants at the flowering differed from that of wild type plants. Thus, we tested whether the increase of the grain yield was mainly caused by the increased AGPase activity during grain filling, or was it mainly caused by the plant size change at the flowering stage. To answer this question, we simulated three scenarios: (1) we changed both the plant size at the flowering stage and $v_{m_grain_Star_syn}$ during grain filling for *Sh2r6hs* transgenic plant; (2)

we changed only the plant size at the flowering stage for *Sh2r6hs* transgenic plant; (3) we changed only $v_{m_grain_Star_syn}$ during grain filling for *Sh2r6hs* transgenic plant. Simulation results matched experimental observations for both the first and the second scenarios, but not for the third scenario (Figure 4e). These data demonstrate that the increased grain yield in *Sh2r6hs* transgenic plants is mainly contributed by change of the plant size at the flowering stage, rather than being contributed by the enhancement of endosperm starch synthesis capacity during grain filling.

Mapping genetic variations of capacities of reaction and diffusion processes to phenotypic variations of grain yield and yield-related agronomic traits

After validating WACNI against experiments under various environmental treatments and genetic manipulations, we used it to explore influence of the capacity of 28 reaction and diffusion processes on eight agronomic traits (Supplementary Figures 4-10). Based on the predicted response patterns of grain yield to parameter changes, we classified the 28 parameters into four categories. Specifically, (1) eleven parameters that can monotonically enhance grain yield were termed as universal yield enhancers (UYEs; shown in Figure 5a); (2) four parameters that can monotonically inhibit grain yield were termed as universal yield inhibitors (UYIs; shown in Figure 5b); (3) six parameters that can non-linearly influence grain yield were termed as conditional yield enhancers (CYEs; shown in Figure 5c); (4) seven parameters having little or no

influence on grain yield were termed as weak yield regulators (WYRs; exemplified in Figure 5d).

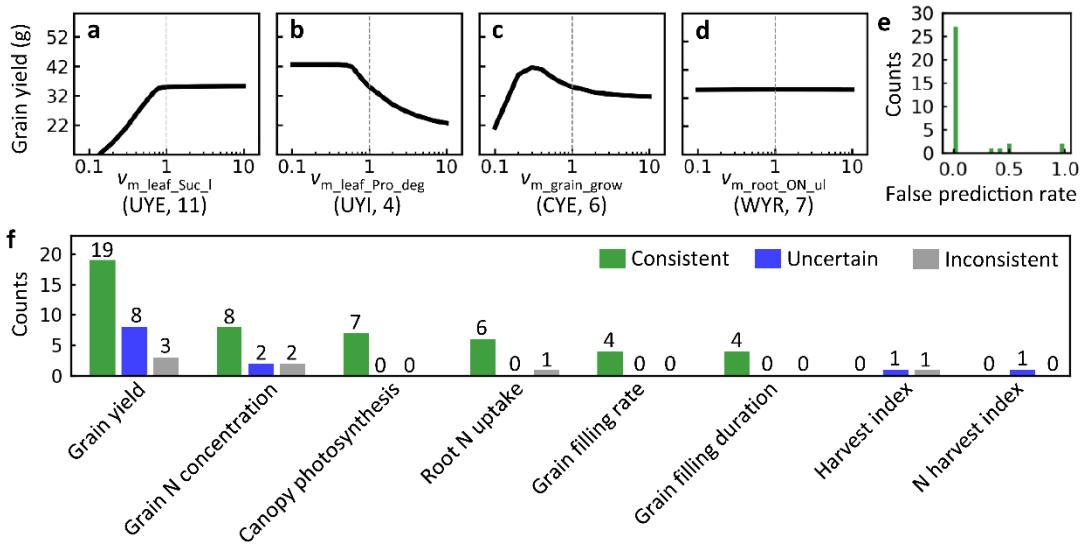

Figure 5. Predicting and grouping the effects of manipulating capacities of 28 reaction and diffusion processes on grain yield and yield-related agronomic traits. **a**, leaf sucrose loading capacity ($v_{m_leaf_Suc_l}$) is an example illustrating a universal yield enhancer which can monotonically increase grain yield when its value ranges from [0.1, 10]-fold to its default value. **b**, leaf protein degradation capacity $v_{m_leaf_Pro_deg}$ is an example illustrating a universal yield inhibitor which can monotonically decrease grain yield. **c**, grain growth capacity $v_{m_grain_grow}$ is an example illustrating a conditional yield enhancer which can non-linearly influence grain yield. **d**, root organic nitrogen unloading capacity $v_{m_root_ON_ul}$ is an example illustrating a weak yield regulator which can hardly influence grain yield. **e**, distribution of false prediction rate on agronomic traits for 33 of the different genetic manipulation cases shown in Supplementary Table 2 with at least one agronomic trait measured. **f**, distribution of consistent, uncertain and inconsistent predictions with experimental observations on eight agronomic traits for genetic manipulations shown in Supplementary Table 2.

We further compiled the genes and QTLs in rice controlling the above 28 parameters published thus far. Thirty-eight genes/QTLs were collected, among which there were

33 manipulations from which at least one of the eight agronomic traits was measured (Supplementary Table 2; see a brief functional description of each gene/QTL in Supplementary Table 3). We emphasize that WACNI had a strong predictive power on the response patterns of agronomic traits by genetic manipulations. For example, WACNI predicted a strong negative impact of impaired $v_{m_leaf_Suc_l}$ on the grain filling rate, the total canopy photosynthesis, the harvest index and the final grain yield; although the grain yield does not decrease with increasing $v_{m_leaf_Suc_l}$, increasing the $v_{m_leaf_Suc_l}$ to be higher than 60% of the default value can no longer increase grain yield (Supplementary Figure 5; Figure 5a). Consistently, it was observed that the impaired function of *OsSUT2*, which exports sugar from the leaves, led to severe growth retardation and yield decrease, whereas higher expression of *OsSUT2* did not result in increased yield compared to that of wild type plants [67]. We further calculated the false prediction rate for each genetic manipulation case. False prediction rate defines the ratio between number of predictions failed to match the experimental observations and the number of all experimentally observed agronomic traits. For example, response patterns of three agronomic traits were measured experimentally (‘T1’, ‘T2’ and ‘T3’) for *OsFd-GOGAT* mutant plants, among which WACNI correctly predicted the response patterns of two (‘T1’ and ‘T3’), but failed to predict the response pattern of ‘T2’ (Supplementary Table 2); in this case, the false prediction rate was 33.3%. In all the 33 genetic manipulation cases, the mean and the median false prediction rates were 11.3% and 0%, respectively (Figure 5e; Supplementary Table 2).

Although none of the above mentioned studies (Supplementary Table 2) measured all the eight agronomic traits (‘T1’-‘T8’) simultaneously, the response patterns of each agronomic trait to different genetic manipulations were predicted with high accuracy across all our measurements (Figure 5f). Specifically, the false prediction rates for eight agronomic traits were 10%, 17%, 0%, 14%, 0%, 0%, 50%, 0%, respectively (‘Inconsistent’ in Figure 5f-m). Besides, non-linear effects of certain genetic manipulations on some agronomic traits exist (Supplementary Figures 4-10). In these cases, the simulation results cannot be determined as consistent with experimental observations from the published work or not, due to the lack of information on numeric values of the manipulated parameters (labelled as ‘Uncertain’ in Figure 5f).

Designing rice physiological ideotype for super-high yield

Finally, WACNI was combined with a genetic algorithm to search the optimal parameter values for maximizing the grain yield. Specifically, we first randomly varied values of specific parameters in a range from 50% to 200% to their default values to generate five independent populations; then we “evolved” these five populations using high grain yield as the selection target. At the end of 100 generations of *in silico* evolution, the highest grain yields in these five populations were found to be similar (Supplementary Figure 11). The top 1% individuals ranking

by the final grain yield in each population were then merged to form an elite plant group (the 'Elite' group in Figure 6b-k and Supplementary Figure 12). In general, values of UYEs were up-regulated, values of UYIs were down-regulated, but the values of CYEs and WYRs did not form any particular pattern (Figure 6a). Although 'Elite' individuals had similar high grain yield, parameter values for these individuals varied. Some parameters were conserved with small variance among 'Elite' individuals, e.g. $v_{m_grain_Star_syn}$, $v_{m_leaf_Pro_deg}$, $v_{m_leaf_ON_l}$ and $v_{m_root_Suc_ul}$; on the contrary, up to a 4-fold differences in values exist for some other parameters, e.g. $v_{m_leaf_N_ass}$, $v_{m_leaf_IN_ul}$, $v_{m_grain_Pro_syn}$ and $v_{m_stem_Pro_syn}$ (Figure 6a-c). The initial partitioning of carbon and nitrogen among organs at the flowering stage for 'Elite' individuals was distinct from the 'Ctrl' individual (individual with default model parameter values), e.g. the grain number increased while the root size decreased dramatically for 'Elite' individuals (Supplementary Figure 12). Overall, the optimization of biochemical and physiological parameters resulted in a remarkable (54%)increase of the grain yield, at the expense of a 37% decrease in grain nitrogen concentration (Figure 6e-f).

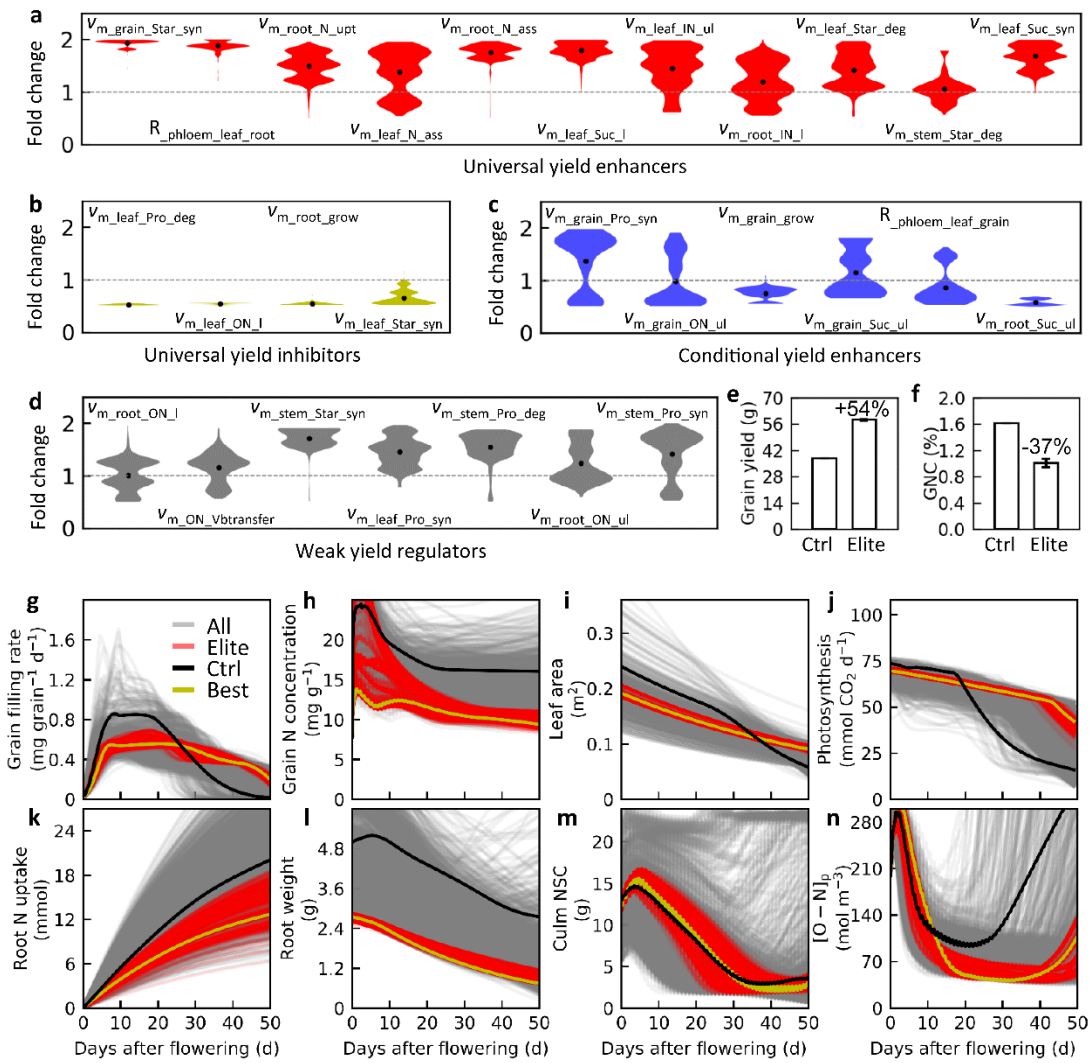

Figure 6. Designing rice physiological ideotype for super-high yield by optimizing the model parameters. Distribution of relative value of each biochemical/physiological parameter (fold change from its default value) for *in silico* high-yield individuals, including universal yield enhancers (**a**), universal yield inhibitors (**b**), conditional yield enhancers (**c**) and weak yield regulators (**d**). Comparison of grain yield per plant (**e**) and grain nitrogen concentration (**f**) for high-yield individuals (n=500, 'Elite') and grain yield of individual with default parameters ('Ctrl'). **g-n**, comparison of macroscopic physiological dynamic changes of the 'Ctrl' individual, the 'Elite' individuals, the 'Best' individual with highest grain yield in 'Elite', and 'All' other individuals generated during *in silico* evolution. See detailed information of parameter values for 'Elite' individuals (a-d) in Supplementary Datasets 1. Abbreviations: NSC, non-structural carbohydrates; $[O\text{-}N]_p$, phloem O-N concentration.

‘Elite’ individuals also show distinct patterns with regard to macroscopic physiological features compared to other individuals. For example, the grain filling rate of ‘Elite’ individuals was relatively low during the first 7 days after flowering, but was moderate between 7 to 25 days after flowering, whereas the rate decreased at much slower pace, starting from 20 days after flowering to the harvest stage, when compared to ‘Ctrl’ and other individuals (Figure 6g). This ‘steady and sustained’ grain filling rate resulted in a nearly linear grain weight gain for the ‘Elite’ individuals rather than the usual sigmoid curve, as for ‘Ctrl’ and other individuals (Supplementary Figure 13). Grain nitrogen concentration was constantly lower during grain filling for the ‘Elite’ individuals (Figure 6h). Further, the ‘Elite’ individuals had slower rate of decrease in both the leaf area as well as in the rate of canopy photosynthesis (Figure 6i-j), a feature commonly known as ‘stay green’ [68]. Surprisingly, ‘Elite’ individuals had a much smaller root mass throughout the grain filling period, and also a lower total root nitrogen uptake (Figure 6k-l). Notably, some ‘Elite’ individuals had similar root nitrogen uptake as the ‘Ctrl’ plants did (Figure 6k), as a result of their higher root nitrogen uptake capacity ($v_{m_root_N_upt}$, Figure 6a). Finally, the ‘Elite’ individuals had similar stem non-structural carbohydrate use pattern as ‘Ctrl’ plants throughout the grain filling period (Figure 6m); on the other hand, the organic nitrogen concentration in phloem ($[O\text{-}N]_p$) was at a low level in the ‘Elite’ individuals starting from 10 days after flowering to the harvest stage; this is in contrast to ‘Ctrl’ and many other plants, where $[O\text{-}N]_p$ dramatically increases during the late grain filling period (Figure 6n).

DISCUSSION

Despite the descriptive research of source sink interaction in single cells or organs, the plant level coordination of processes in different source and sink organs has been largely disregarded during crop improvement research; this has been due to difficulties in the interpretation of such a complex network [29]. Crop systems models have been used in designing agronomic practices [69,70], testing hypotheses regarding the responses of crops to climate change [71,72], guiding selection of traits for breeding [73] and assessing different strategies to adapt to future climate change [74]. Here, we have introduced a mechanistic model that accurately predicts plant level source sink interactions during grain filling, as an emergent property, from basic biochemical and physiological processes in different plant organs (Figure 1); this clearly differs from the mainstream approaches using either preset rules on the relationship between the source and sink organs, or the empirical correlation derived from the measured data.

Considering the numerous processes within different organs and the extensive metabolite exchange between organs, it is remarkable that WACNI accurately predicts physiological changes of a rice plant during the grain filling period both under normal condition as well as under various field practices and/or environmental perturbations (Figures 2-3). Further analysis using WACNI confirms many conjectures raised over

the past decades on high-yield crop breeding and crop source-sink relations. For example, functional ‘stay green’ of leaves, higher leaf sucrose export rate, higher endosperm starch synthesis capacity and more efficient remobilization of stem starch reserves are among the major means considered for increasing crop yield (Figure 6a, i, j, m)[75-78]. Moreover, WACNI systematically evaluates the reported impact on agronomic traits of genetic manipulations of source, transport and sink related properties (Figures 4-5; Supplementary Table 2). In particular, WACNI correctly predicts 64-100% of the responses to all 33 genetic manipulations, for six out of eight major agronomic traits, with the remaining two traits, harvest index and nitrogen harvest index, having very low (only 1 to 2) number of reported values (Figure 5f) and hence cannot be properly evaluated. All these results demonstrate that WACNI is a robust mechanistic model linking genotypic variation to phenotypic variation under different environments.

Besides its mechanistic basis, another major feature that confers the high prediction accuracy of WACNI is its parameterization routine. Parameterization of WACNI relies on extensive literature survey (Supplementary Table 1) , resulting in a primary reference dataset on natural variation of important rice traits, which can be constantly updated to support systems modeling of rice metabolism, growth and development. It is also worth mentioning here that since most processes described in WACNI are rather generic among plants, WACNI can be adapted and parameterized for other

plants, especially for cereal crops. In addition, WACNI follows a principle of modular design, that is, the metabolic processes involved in leaf, grain, root, and stem are modeled in individual modules, which can easily be replaced by other modules or extended by other researchers whenever needed. This feature enables WACNI to be a framework to support future crop systems models development, e.g. in developing models of plant signaling transduction or hormone regulation [79] and more elaborate models combining 3D root/shoot morphogenesis, development and functions [80-82].

Plant growth and developmental processes are ultimately supported by the metabolic processes in different organs and fluxes between organs, establishing a map of the carbon and nitrogen fluxes within a whole plant has been a major challenge of plant biology [83]. Here, for the first time, we quantify the entire carbon and nitrogen budget within a rice plant during the grain filling period using WACNI (Figure 2g). The map drawn here opens new research opportunities. For example, we can use it in evaluating how resource partitioning among sink organs influences the overall efficiency of the whole system; furthermore, it can be used to precisely calculate contribution from each source tissue to sink development. WACNI therefore provides a theoretical tool to enable detailed study on controls and even genetic basis of carbon and nitrogen fluxes in a plant. It is exciting to see the availability of comprehensive datasets on whole plant level metabolic fluxes based on fluxomics [84].

Model guided enhancement of photosynthetic efficiency has gained major success in recent years [2,40,42]. Being able to link molecular level processes to physiological changes all the way up to agronomic traits, WACNI, for the first time, offers an opportunity to design features associated with super high yield. Optimization of source sink and transport related processes, based on WACNI prediction, show that the rice grain yield potential can reach 21 t ha^{-1}, given that the water content is 13.5% and husks account for 20% of weight in rough rice (Figure 6e). This is 40% higher than the current highest record of rice grain yield [85]. Analysis based on WACNI simulations suggests that to reach such a high yield one option is to have a dry weight of ~22 mg per dehulled grain, a total number of filled spikelets being ~$6.7*10^8$ ha^{-1} (Supplementary Datasets 1). In such a rice line, a balanced source sink relation is needed to support 'stay green' of leaves and maximize both instantaneous and long-term canopy photosynthesis, which together realize the 'steady and sustained' grain filling rate till 50 days after flowering (Figure 6g). Many previously identified genes, being either UYEs, UYIs, CYEs, can be used as targets of fine-tuning to control carbon and nitrogen fluxes between different organs to realize the required physiological features, ultimately leading to the designed high yield potential (Supplementary Table 2).

Methods

Model development

The model developed here was depicted diagrammatically in Figure 1. The individual modules were developed following the basic procedure as in Zhu, et al. [86]. Essentially, after the reaction diagrams were established, differential equations, rate equations, and algebraic equations representing conserved quantities were developed. The model was implemented in MATLAB and solved using ode15s (the MathWorks Inc., Natick, MA, USA). WACNI computed changes in the metabolite concentrations by the differences between rates of fluxes generating and consuming metabolites.

Fourteen different types of primary biochemical/biophysical processes were incorporated in WACNI (Figure 1). The rate equations were described in four different subsections according to the organs they present in, i.e., root, leaf, grains and stem (including culm and sheath) in the following (Eqn 1.1-14.1). Respiration for each organ was described in the subsequent *Respiration* subsection (Eqn 15.1-15.4).

Root

I-N uptake and assimilation: Two I-N uptake systems present in roots, i.e., the high affinity transport system (HATS) and the low affinity transport system (LATS); which together ensure I-N uptake at different soil N concentrations [87]. The uptake rates of HATS and LATS were modeled with Michaelis-Menten kinetics model and linear model, respectively (Eqn 1.2). Sugar level also influences mineral transport as sugar provides energy needed for these processes [88,89]. The impact of root sucrose level on I-N uptake was modelled with a Monod function [90], i.e., the first item of Eqn (1.2). Root total N concentration has a feedback inhibitory effect ($\alpha_{N_inhibit}$) on root HATS [87]. Finally, these regulatory processes were incorporated into a single root I-N uptake equation to calculate total root I-N uptake rate ($v_{root_N_upt}$):

$$\alpha_{N_inhibit} = \begin{cases} 1 - \dfrac{[N]_{root}}{[N]_{inhibit_up}}, [N]_{root} < [N]_{inhibit_up} \\ 0, [N]_{root} \geq [N]_{inhibit_up} \end{cases} \quad (1.1)$$

$$v_{\text{root_N_upt}} = \frac{[\text{Suc}]_{\text{root}}}{K_{\text{m1}} + [\text{Suc}]_{\text{root}}} \cdot (\alpha_{\text{N_inhibit}} \cdot v_{\text{m_root_HATS}} \cdot \frac{[\text{I-N}]_{\text{soil}}}{K_{\text{m2}} + [\text{I-N}]_{\text{soil}}} + k_{\text{root_LATS}} \cdot [\text{I-N}]_{\text{soil}}) \quad (1.2)$$

in which $[\text{I-N}]_{\text{soil}}$ is soil I-N concentration, $[\text{Suc}]_{\text{root}}$ is root sucrose concentration, $[\text{N}]_{\text{root}}$ is total root N concentration (including I-N and O-N). $[\text{N}]_{\text{inhibit_up}}$ is upper limit of total root N concentration above which N uptake by HATS ceases, K_{m1} and K_{m2} are Michaelis-constants, $v_{\text{m_root_HATS}}$ is root HATS maximal I-N uptake rate, $k_{\text{root_LATS}}$ is root LATS I-N uptake rate coefficient (Supplementary Table 1).

Root N assimilation depends on energy and reducing power derived from sugar [91]. Hence, root I-N assimilation rate ($v_{\text{root_N_ass}}$) was modelled based on $[\text{Suc}]_{\text{root}}$ and $[\text{I-N}]_{\text{root}}$:

$$v_{\text{root_N_ass}} = v_{\text{m_root_N_ass}} \cdot \frac{[\text{Suc}]_{\text{root}}}{K_{\text{m3}} + [\text{Suc}]_{\text{root}}} \cdot \frac{[\text{I-N}]_{\text{root}}}{K_{\text{m4}} + [\text{I-N}]_{\text{root}}} \quad (2.1)$$

in which K_{m3} and K_{m4} are Michaelis-constants, $v_{\text{m_root_N_ass}}$ is root maximal I-N assimilation rate (Supplementary Table 1).

Root growth: As sugar supply is a major factor limiting root growth [92], and organ growth rate is positively correlated with sugar level in the organ before reaching its maximal capacity [92-94], a critical sucrose concentration ($[\text{Suc}]_{\text{grow_low}}$) was set, below which root growth ceased. A Monod function was applied to describe the relation between root sucrose level and its growth rate ($v_{\text{root_grow}}$):

$$v_{\text{root_grow}} = \begin{cases} 0, [\text{Suc}]_{\text{root}} < [\text{Suc}]_{\text{grow_low}} \\ v_{\text{m_root_grow}} \cdot \dfrac{[\text{Suc}]_{\text{root}} - [\text{Suc}]_{\text{grow_low}}}{K_{\text{m5}} + ([\text{Suc}]_{\text{root}} - [\text{Suc}]_{\text{grow_low}})}, [\text{Suc}]_{\text{root}} \geq [\text{Suc}]_{\text{grow_low}} \end{cases} \quad (3.1)$$

in which K_{m5} is Michaelis-constant, $v_{\text{m_root_grow}}$ is the root maximal relative growth rate (Supplementary Table 1).

Root senescence: Root loss during senescence was modelled based on two factors, aging and carbohydrate supply. Specifically, there is a minimal (constant) relative senescence rate $\alpha_{\text{sene_root}}$ (Supplementary Table 1) due to aging of root [95,96], but when sucrose concentration is lower than a critical level ($[\text{Suc}]_{\text{sene_up}}$), root senescence rate ($v_{\text{root_sene}}$) would be accelerated as a result of carbohydrate starvation [97]:

$$v_{\text{root_sene}} = \begin{cases} \alpha_{\text{root_sene}} \cdot e^{-\beta_{\text{root_sene}} \cdot ([\text{Suc}]_{\text{root}} - [\text{Suc}]_{\text{sene_up}})}, [\text{Suc}]_{\text{root}} < [\text{Suc}]_{\text{sene_up}} \\ \alpha_{\text{root_sene_}}, [\text{Suc}]_{\text{root}} \geq [\text{Suc}]_{\text{sene_up}} \end{cases} \quad (4.1)$$

in which $\beta_{\text{root_sene}}$ is an empirical coefficient (Supplementary Table 1).

Leaf

Photosynthesis and N assimilation: Leaf level light reaction, Calvin-Benson cycle and photorespiration were modelled based on the Farquhar-von Caemmerer-Berry (FvB) model [98]. To scale up them to a canopy level, a sun-shade model described in De Pury and Farquhar [99] was used (see below).

Leaf protein level (especially the level of enzyme Rubisco, which accounts for major leaf protein) has been shown to be linearly and positively correlated with leaf light reaction and dark reaction activity before reaching their maximal capacity in many experiments [100,101], while leaf non-structural carbohydrates (NSC, refer to sucrose and starch in the current model) accumulation can inhibit photosynthesis [102] through multiple feedback regulatory pathways [103,104]. These effects were considered by setting an activation coefficient ($\alpha_{\text{Pro_promote}}$, Eqn 5.1) of leaf protein content ($[\text{Pro}]_{\text{leaf}}$) and an inhibition coefficient ($\alpha_{\text{NSC_inhibit}}$, Eqn 5.2) of leaf NSC content ($[\text{NSC}]_{\text{leaf}}$) to parameters involved in both photosynthetic electron transport rate v_J and potential CO_2 assimilation rate v_{A0} (Eqn 5.3-5.8):

$$\alpha_{\text{Pro_promote}} = \begin{cases} \dfrac{[\text{Pro}]_{\text{leaf}}}{[\text{Pro}]_{\text{promote_up}}}, [\text{Pro}]_{\text{leaf}} < [\text{Pro}]_{\text{promote_up}} \\ 1, [\text{Pro}]_{\text{leaf}} \geq [\text{Pro}]_{\text{promote_up}} \end{cases} \quad (5.1)$$

$$\alpha_{\text{NSC_inhibit}} = \begin{cases} 1, [\text{NSC}]_{\text{leaf}} < [\text{NSC}]_{\text{inhibit_low}} \\ 1 - \dfrac{[\text{NSC}]_{\text{leaf}} - [\text{NSC}]_{\text{inhibit_low}}}{[\text{NSC}]_{\text{inhibit_up}} - [\text{NSC}]_{\text{inhibit_low}}}, [\text{NSC}]_{\text{inhibit_low}} \leq [\text{NSC}]_{\text{leaf}} \leq [\text{NSC}]_{\text{inhibit_up}} \\ 0, [\text{NSC}]_{\text{leaf}} > [\text{NSC}]_{\text{inhibit_up}} \end{cases}$$

(5.2)

$$v_{\text{cmax}} = \alpha_{\text{Pro_promote}} \cdot \alpha_{\text{NSC_inhibit}} \cdot v_{\text{cmax0}} \quad (5.3)$$

$$J_{\text{max}} = \alpha_{\text{Pro_promote}} \cdot \alpha_{\text{NSC_inhibit}} \cdot J_{\text{max0}} \quad (5.4)$$

$$\theta = \alpha_{\text{Pro_promote}} \cdot \theta_0 \quad (5.5)$$

$$\varphi = \alpha_{\text{Pro_promote}} \cdot \varphi_0 \tag{5.6}$$

$$v_{\text{A0}} = v_{\text{cmax}} \cdot \frac{[\text{CO}_2]_{\text{i}} - \Gamma}{K_{\text{m6}} + [\text{CO}_2]_{\text{i}}} \tag{5.7}$$

$$v_{\text{J}} = \frac{\varphi \cdot I + J_{\max} - \sqrt{(\varphi \cdot I + J_{\max})^2 - 4 \cdot \varphi \cdot \theta \cdot I \cdot J_{\max}}}{2\theta} \tag{5.8}$$

in which K_{m6} is Michaelis-constant; $[\text{Pro}]_{\text{promote_up}}$, $[\text{NSC}]_{\text{inhibit_up}}$ and $[\text{NSC}]_{\text{inhibit_low}}$ are critical leaf protein and NSC content; φ_0=0.85*0.5 and θ_0=0.7 are empirical constants [98]; v_{cmax0} is the potential maximal Rubisco carboxylation rate, J_{max0} is the potential maximal electron transport rate (Supplementary Table 1); Γ is CO_2 compensation point in the absence of mitochondrial respiration (Supplementary Table 1). I is irradiance absorbed by leaves. Whole-plant I, v_{cmax0} and J_{max0} were calculated separately for sunlit and shaded leaves, e.g. I_{sun}, I_{sh}, $v_{\text{cmax0_sun}}$, $v_{\text{cmax0_sh}}$, $J_{\text{max0_sun}}$ and $J_{\text{max0_sh}}$ in Eqn 5.14-5.19, and $v_{\text{_leaf_N_ass0}}$ in Eqn 5.23, based on light extinction profile within the canopy throughout the day following De Pury and Farquhar [99]:

$$\delta = -23.4 \frac{\pi}{180} \cos \frac{2\pi(\text{DOY}+10)}{365} \tag{5.9}$$

$$\sin \beta = \sin \lambda \cdot \sin \delta + \cos \lambda \cdot \cos \delta \cdot \cos \frac{\pi \cdot (\tau - 12)}{12} \tag{5.10}$$

$$f_d = \frac{1 - a^{1/\sin \beta}}{1 + a^{1/\sin \beta}(1/f_a - 1)} \tag{5.11}$$

$$L_{\text{C_sun}} = \frac{1 - e^{-k_b \cdot L_{\text{C}}}}{k_b}(1 - e^{-k_b \cdot L_{\text{C}}}) \tag{5.12}$$

$$I_{\text{C}} = \int_0^{L_{\text{C}}} I_l dl = (1 - \rho_{cb}) \cdot I_b \cdot (1 - e^{-k_b' \cdot L_{\text{C}}}) + (1 - \rho_{cd}) \cdot I_d \cdot (1 - e^{-k_d' \cdot L_{\text{C}}}) \tag{5.13}$$

$$\begin{aligned} I_{\text{sun}} = \int_0^{L_{\text{C}}} I_{l_\text{sun}} \cdot f_{l_\text{sun}} dl &= I_b \cdot (1-\sigma) \cdot (1 - e^{-k_b \cdot L_{\text{C}}}) + I_d \cdot (1 - \rho_{cd}) \cdot (1 - e^{(-k_d' + k_b) \cdot L_{\text{C}}}) \cdot \frac{k_d'}{k_d' + k_b} \\ &+ I_b \cdot (1 - \rho_{cb}) \cdot (1 - e^{(-k_b' + k_b) \cdot L_{\text{C}}} \cdot \frac{k_b'}{k_b' + k_b}) - (1-\sigma) \cdot \frac{1 - e^{-2k_b \cdot L_{\text{C}}}}{2} \end{aligned} \tag{5.14}$$

$$I_{\mathrm{sh}} = I_{\mathrm{C}} - I_{\mathrm{sun}} \tag{5.15}$$

$$v_{\mathrm{cmax0_sun}} = v_{\mathrm{cmax0}} \cdot L_{\mathrm{C_sun}} \tag{5.16}$$

$$J_{\mathrm{max0_sun}} = J_{\mathrm{max0}} \cdot L_{\mathrm{C_sun}} \tag{5.17}$$

$$v_{\mathrm{cmax0_sh}} = v_{\mathrm{cmax0}} \cdot (L_{\mathrm{C}} - L_{\mathrm{C_sun}}) \tag{5.18}$$

$$J_{\mathrm{max0_sh}} = J_{\mathrm{max0}} \cdot (L_{\mathrm{C}} - L_{\mathrm{C_sun}}) \tag{5.19}$$

in which δ is solar declination angle; DOY is current day of year; β is solar elevation angle; λ is latitude of experimental base; τ is local time of day; f_d is fraction of diffuse irradiance; f_a=0.425 is forward scattering coefficient of PAR in atmosphere; a=0.75 is atmospheric transmission coefficient of PAR; L_{c} is canopy leaf area index; $L_{\mathrm{c_sun}}$ is the sunlit leaf area index; $k_b=k_{b0}/\sin\beta$ is beam radiation extinction coefficient of canopy; $k'_b=0.9k_b$ is beam and scattered beam PAR extinction coefficient; k_d=0.78 is diffuse PAR extinction coefficient; $k'_d=0.9k_d$ is diffuse and scattered diffuse PAR extinction coefficient; I_0 is total incident PAR intensity at top of canopy; $I_d=I_0 \cdot f_d$ is diffuse PAR intensity; $I_b=I_0 \cdot (1-f_d)$ is beam PAR intensity; I_{C} is irradiance absorbed by the canopy; I_{sun} is irradiance absorbed by the sunlit leaves; I_{sh} is irradiance absorbed by the shaded leaves; ρ_{cb}=0.029 is canopy reflection coefficient for beam PAR; ρ_{cd}=0.036 is canopy reflection coefficient for diffuse PAR; σ=0.15 is leaf scattering coefficient of PAR. More detailed information of these processes and parameters can be found in De Pury and Farquhar [99].

Intercellular CO_2 concentration ($[CO_2]_i$) is determined by ambient CO_2 concentration ($[CO_2]_a$), leaf stomatal conductance (g_s) and leaf net photosynthetic rate (A - R_{leaf}):

$$[\mathrm{CO_2}]_{\mathrm{i}} = [\mathrm{CO_2}]_{\mathrm{a}} - \frac{A - R_{\mathrm{leaf}}}{g_{\mathrm{s}}} \tag{5.20}$$

in which leaf gross photosynthetic rate A is calculated in Eqn (5.27), and respiration rate R_{leaf} is calculated in the following *Respiration* subsection.

Leaf stomatal conductance (g_s) is influenced by many factors, e.g. CO_2 concentration, vapor pressure deficit, light intensity, leaf water potential, temperature and abscisic acid concentration [105-107]. Diffusion of CO_2 from ambient air to intercellular space was modeled following Leuning [108]:

$$g_s = g_0 + a_1 \cdot \frac{A}{[CO_2]_i - \Gamma} \cdot \frac{1}{1 + \frac{VPD_{leaf}}{VPD_0}} \quad (5.21)$$

in which g_0=0.01 is residual stomatal conductance, a_1=20 and VPD_0=0.35 are empirical constants [108]. Leaf vapor pressure deficit (VPD_{leaf}) is the difference between leaf vapor pressure (which is assumed to be saturated and determined by leaf temperature T) and actual air vapor pressure (which is determined by relative air humidity RH_{air}), and was calculated following Allen, et al. [109]:

$$VPD_{leaf} = 0.6108 \exp[\frac{17.27T}{T + 237.3}] \cdot (1 - RH_{air}) \quad (5.22)$$

As photosynthetic light reaction generates abundant ATP and reducing power (e.g. NADPH and Ferredoxin), which are necessary for I-N assimilation, leaf acts as a major N assimilator as well as root [110]. Potential I-N assimilation rate (v_{N_ass0}) was modeled based on leaf protein level and I-N concentration ($[\text{I-N}]_{leaf}$):

$$v_{leaf_N_ass0} = \alpha_{Pro_promote} \cdot v_{m_leaf_N_ass} \cdot \frac{[\text{I-N}]_{leaf}}{K_{m7} + [\text{I-N}]_{leaf}} \quad (5.23)$$

in which K_{m7} is Michaelis-constant, $v_{m_leaf_N_ass}$ is leaf maximal N assimilation rate (Supplementary Table 1).

Calvin cycle, photorespiration and I-N assimilation compete for reducing power derived from light reaction when light is limiting [111]. Light reaction derived reducing power producing rate (v_{NADPH_p}) was calculated as following:

$$v_{NADPH_p} = \frac{v_J}{2} \quad (5.24)$$

Calvin cycle and photorespiration consume 2 NADPH per cycle, and average I-N assimilation consumes 3 NADPH per N (if NO_3^- is the N source, it needs 5 NADPH or equivalent reduction power; if NH_4^+ is the N source, it needs 1 NADPH or equivalent reduction power) [112]. Thus the potential NADPH consume rate (v_{NADPH_c0}) was calculated as following:

$$v_{NADPH_c0} = 2v_{cmax} \cdot \frac{[CO_2]_i + \Gamma}{K_{m6} + [CO_2]_i} + 3v_{leaf_N_ass0} \quad (5.25)$$

The actual CO_2 assimilation rate A and I-N assimilation rate ($v_{leaf_N_ass}$) were finally

determined by balancing NADPH production and consumption:

$$\delta = \begin{cases} \dfrac{v_{\text{NADPH_p}}}{v_{\text{NADPH_c0}}}, v_{\text{NADPH_p}} < v_{\text{NADPH_c0}} \\ 1, v_{\text{NADPH_p}} \geq v_{\text{NADPH_c0}} \end{cases} \quad (5.26)$$

$$A = \delta \cdot v_{\text{A0}} \quad (5.27)$$

$$v_{\text{leaf_N_ass}} = \delta \cdot v_{\text{leaf_N_ass0}} \quad (5.28)$$

Final CO_2 and I-N assimilation rate were determined by solving the above equations (Eqn 5.1-5.28).

Leaf C and N substrates homeostasis: During the day, photosynthetic derived triose phosphates (TP) convert to sucrose ($v_{\text{leaf_Suc_syn}}$) and starch ($v_{\text{leaf_Star_syn}}$) synchronously:

$$v_{\text{leaf_Suc_syn}} = v_{\text{m_leaf_Suc_syn}} \cdot \frac{[\text{TP}]_{\text{leaf}} - \dfrac{[\text{Suc}]_{\text{leaf}}}{K_{\text{e1}}}}{K_{\text{m8}} + [\text{TP}]_{\text{leaf}}} \quad (6.1)$$

$$v_{\text{leaf_Star_syn}} = v_{\text{m_leaf_Star_syn}} \cdot \frac{[\text{TP}]_{\text{leaf}}}{K_{\text{m9}} + [\text{TP}]_{\text{leaf}}} \quad (6.2)$$

in which K_{m8}, K_{m9} and K_{e1} are Michaelis-constants, $v_{\text{m_leaf_Suc_syn}}$ is leaf maximal sucrose synthesis (TP to sucrose conversion) rate and $v_{\text{m_leaf_Star_syn}}$ is leaf maximal starch synthesis (TP to starch conversion) rate (Supplementary Table 1).

In night, sucrose level decreases and daily synthesized starch degrades gradually [113]. There are a number of models simulating nighttime starch degradation, most of which incorporate a circadian clock control of the process [114-116]. For simplification, we used a simple substrates feedback regulation mechanism to simulate starch degradation rate ($v_{\text{leaf_Star_deg}}$):

$$v_{\text{leaf_Star_deg}} = \begin{cases} v_{\text{m_leaf_Star_deg}} \cdot \dfrac{[\text{Star}]_{\text{leaf}}}{K_{\text{m10}} + [\text{Star}]_{\text{leaf}}} \cdot \dfrac{[\text{Suc}]_{\text{leaf_Star_deg_low}} - [\text{Suc}]_{\text{leaf}}}{[\text{Suc}]_{\text{leaf_Star_deg_low}} + [\text{Suc}]_{\text{leaf}}}, [\text{Suc}]_{\text{leaf}} < [\text{Suc}]_{\text{leaf_Star_deg_low}} \\ 0, [\text{Suc}]_{\text{leaf}} \geq [\text{Suc}]_{\text{leaf_Star_deg_low}} \end{cases}$$

(6.3)

in which K_{m10} is Michaelis-constant, $[\text{Suc}]_{\text{leaf_Star_deg_low}}$ is critical leaf sucrose

concentration below which starch starts to decompose, $v_{\text{m_leaf_Star_deg}}$ is leaf maximal starch degradation rate (Supplementary Table 1).

Leaf O-N and protein are in dynamic balance by their inter-conversion (conversion rate $v_{\text{leaf_O-N2Pro}} > 0$ means a conversion from O-N to protein, and *vice versa*):

$$v_{\text{leaf_O-N2Pro}} = \begin{cases} v_{\text{m_leaf_Pro_syn}} \cdot \dfrac{[\text{O-N}]_{\text{leaf}} - [\text{O-N}]_{\text{leaf_Pro_syn_low}}}{K_{\text{m11}} + [\text{O-N}]_{\text{leaf}}}, [\text{O-N}]_{\text{leaf}} > [\text{O-N}]_{\text{leaf_Pro_syn_low}} \\ -v_{\text{m_leaf_Pro_deg}} \cdot \dfrac{[\text{O-N}]_{\text{leaf_Pro_syn_low}} - [\text{O-N}]_{\text{leaf}}}{K_{\text{m11}} + [\text{O-N}]_{\text{leaf}}}, [\text{O-N}]_{\text{leaf}} \le [\text{O-N}]_{\text{leaf_Pro_syn_low}} \end{cases} \quad (7.1)$$

in which K_{m11} is Michaelis-constant, $[\text{O-N}]_{\text{leaf_Pro_syn_low}}$ is critical leaf O-N concentration below which protein synthesis ceases and starts to decompose, $v_{\text{m_leaf_Pro_syn}}$ is leaf maximal protein synthesis rate and $v_{\text{m_leaf_Pro_deg}}$ is leaf maximal protein degradation rate (Supplementary Table 1).

Leaf senescence: Similar to that of root, there is a minimal (constant) relative leaf photosynthetic area (S_{leaf}) loss rate $\alpha_{\text{leaf_sene}}$ (Supplementary Table 1) due to aging [117]. As leaf senescence is closely related to leaf N remobilization during grain filling [118,119], we proposed that leaf senescence rate ($v_{\text{leaf_sene}}$) would be accelerated as a result of nitrogen starvation when leaf total nitrogen level ($[\text{N}]_{\text{leaf}}$; including I-N, O-N and protein) decreased below a critical level $[\text{N}]_{\text{sene_up}}$:

$$v_{\text{leaf_sene}} = \begin{cases} \alpha_{\text{leaf_sene}} \cdot e^{-\beta_{\text{leaf_sene}} \cdot ([\text{N}]_{\text{leaf}} - [\text{N}]_{\text{sene_up}})}, [\text{N}]_{\text{leaf}} < [\text{N}]_{\text{sene_up}} \\ \alpha_{\text{leaf_sene}}, [\text{N}]_{\text{leaf}} \ge [\text{N}]_{\text{sene_up}} \end{cases} \quad (8.1)$$

in which $\beta_{\text{leaf_sene}}$ is an empirical coefficient (Supplementary Table 1).

Grains

In WACNI, grain volume expansion and grain filling occur simultaneously rather than being divided into two distinct phases, as it has been reported in both maize and rice that time for expression of enzymes envolved in these two processes is overlaped, and protein/starch granuals are presented in endosperm cells at the very beginning of the grain filling period [120-124].

Grain volume growth: Grain volume growth, i.e., grain cell division, was modelled based on current grain surface area since cell division occurs mainly within several

outer layer cells of grain [125]. Assuming that developing grains has an ellipsoid shape with the width, height and length being w, w and $w \cdot r$ (r is grain length width ratio, Supplementary Table 1), respectively, grain volume (V_{grain}) and grain surface area (S_{grain}) were estimated as following:

$$V_{grain} = \frac{4}{3}\pi \cdot w^3 \cdot r \quad (9.1)$$

$$S_{grain} \approx 4\pi\left(\frac{1+2r^{1.6075}}{3}\right)^{\frac{1}{1.6075}} \cdot w^2 \quad (9.2)$$

Glume size (V_{glume}) and/or and pericarp size can physically restrict expansion of developing grain [126], although the strength of constraint may differ among species [127]. This constraint effect ($\alpha_{restrict}$) was modelled as following:

$$\alpha_{restrict} = \begin{cases} 1, V_{grain} < (1-\varepsilon) \cdot V_{glume_max} \\ \frac{1}{\varepsilon}\left(1 - \frac{V_{grain}}{V_{glume_max}}\right), V_{grain} \geq (1-\varepsilon) \cdot V_{glume_max} \end{cases} \quad (9.3)$$

in which $(1-\varepsilon) \cdot V_{glume}$ is a critical grain volume above which grain expansion will be more and more physically restrained.

In addition, grain volume expansion was modelled based on current grain surface area (S_{grain}) since cell division occurs mainly within several outer layer cells of grain [125]. We further proposed that grain volume expansion rate (v_{grain_grow}) was co-determined by carbohydrate and nitrogen supply, i.e., concentration of sucrose and nitrogen in grain aqueous space ($[\text{O-N}]_{grain}$ and $[\text{Suc}]_{grain}$, respectively) in WACNI:

$$v_{grain_grow} = \alpha_{restrict} \cdot v_{m_grain_grow} \cdot S_{grain} \frac{[\text{O-N}]_{grain}}{K_{m12} + [\text{O-N}]_{grain}} \cdot \frac{[\text{Suc}]_{grain}}{K_{m13} + [\text{Suc}]_{grain}} \quad (9.4)$$

in which K_{m12} and K_{m13} are Michaelis-constants, $v_{m_grain_grow}$ is grain maximal growth rate (Supplementary Table 1).

Grain starch and protein storage: The aqueous space volume (V_{grain_aq}) expands with endosperm cells division and reduces by storage starch and protein (which are insoluble) cumulation:

$$V_{grain_aq} = V_{grain} - \frac{m_{grain_Star}}{\rho_{Star}} - \frac{m_{grain_Pro}}{\rho_{Pro}} \quad (10.1)$$

in which V_{grain} is total grain volume, m_{grain_Star} and m_{grain_Pro} are biomass and ρ_{Star} and ρ_{Pro} are density of cumulated starch and protein in grain, respectively.

For grain filling, storage starch and protein synthesis rate ($v_{grain_Star_syn}$ and $v_{grain_Pro_syn}$) were modeled based on sucrose and O-N concentrations in grain aqueous space following a Michaelis-Menten equation:

$$v_{grain_Star_syn} = v_{m_grain_Star_syn} \cdot \frac{[Suc]_{grain}}{K_{m14} + [Suc]_{grain}} \quad (10.2)$$

$$v_{grain_Pro_syn} = v_{m_grain_Pro_syn} \cdot \frac{[O\text{-}N]_{grain}}{K_{m15} + [O\text{-}N]_{grain}} \quad (10.3)$$

in which K_{m14} and K_{m15} are Michaelis-constants, $v_{m_grain_Star_syn}$ is grain maximal starch synthesis rate, $v_{m_grain_Pro_syn}$ is grain maximal protein synthesis rate (Supplementary Table 1).

Stem

Stem sucrose and starch, O-N and protein homeostasis: Sucrose and starch, O-N and protein are in dynamic balance in stem (including culm and sheath) as a result of inter-conversion between them, respectively. The conversion rates between them ($v_{stem_Suc2Star}$ and $v_{stem_O\text{-}N2Pro}$) were modeled as following:

$$V_{SSP_aq} = SV0 - \frac{m_{SSP_Star}}{\rho_{Star}} - \frac{m_{SSP_Pro}}{\rho_{Pro}} \quad (11.1)$$

$$v_{SSP_Star_syn} = \begin{cases} v_{m_SSP_Star_syn} \cdot \dfrac{[Suc]_{SSP} - [Suc]_{SSP_Star_syn_low}}{K_{m16} + [Suc]_{SSP} - [Suc]_{SSP_Star_syn_low}}, [Suc]_{SSP} > [Suc]_{SSP_Star_syn_low} \\ v_{m_SSP_Star_deg} \cdot \dfrac{[Star]_{SSP}}{K_{m17} + [Suc]_{SSP}} \cdot \dfrac{[Suc]_{SSP} - [Suc]_{SSP_Star_syn_low}}{K_{m16} + [Suc]_{SSP} - [Suc]_{SSP_Star_syn_low}}, [Suc]_{SSP} \le [Suc]_{SSP_Star_syn_low} \end{cases} \quad (11.2)$$

$$v_{SSP_O\text{-}N2Pro} = \begin{cases} v_{m_SSP_Pro_syn} \cdot \dfrac{[O\text{-}N]_{SSP} - [O\text{-}N]_{SSP_Pro_syn_low}}{K_{m18} + [O\text{-}N]_{SSP} - [O\text{-}N]_{SSP_Pro_syn_low}}, [O\text{-}N]_{SSP} > [O\text{-}N]_{SSP_Pro_syn_low} \\ -v_{m_SSP_Pro_deg} \cdot \dfrac{[Pro]_{SSP}}{K_{m19} + [Pro]_{SSP}} \cdot \dfrac{[O\text{-}N]_{SSP} - [O\text{-}N]_{SSP_Pro_syn_low}}{K_{m18} + [O\text{-}N]_{SSP} - [O\text{-}N]_{SSP_Pro_syn_low}}, [O\text{-}N]_{SSP} \le [O\text{-}N]_{SSP_Pro_syn_low} \end{cases}$$

(11.3)

in which V_{stem_aq} is aqueous space volume of stem; m_{stem_Star} and m_{stem_Pro} are biomass of starch and protein in stem, respectively; K_{m16}, K_{m17} K_{m18} and K_{m19} are Michaelis-constants; $v_{m_stem_Star_syn}$ and $v_{m_stem_Star_deg}$ are stem maximal starch synthesis and starch degradation rate, $v_{m_stem_Pro_syn}$ and $v_{m_stem_Pro_deg}$ are stem maximal protein synthesis and protein degradation rate, respectively (Supplementary Table 1).

Xylem and phloem transport: Phloem transport includes short distance transport that occurs at source or sink ends, i.e., material loading or unloading, and long distance transport along phloem sieve tubes. According to Münch's theory, phloem long distance transport resistance is mainly determined by the physical property of the sieve tube and fluid in it. However, transporter proteins, whose efficiency is mainly determined by Michaelis-Menten kinetics, usually control the resistance of short distance transport. As solutes in xylem move with transpiration flow, which is not explicitly considered in our current model, solutes were assumed to be uniformly distributed along xylem path without concentration gradient. For phloem, we divided it into three different compartments and considered the transport resistance between them (see below).

Flux between different phloem compartments: Phloem path was divided into three compartments (see Figure 1), i.e., leaf phloem, grain phloem and root phloem. Flux in phloem is driven by osmotic pressure difference between source and sink according to Münch theory. Sucrose and amino acids are the main osmotic components in phloem [128]. Flux rate ($v_{phloem_flux_leaf_X}$) between phloem compartments of leaf and organ X (X can be grain or root) was modeled as following:

$$v_{phloem_flux_leaf_X} = \frac{([Suc]_{leaf_phloem} + [O\text{-}N]_{leaf_phloem}) - ([Suc]_{X_phloem} + [O\text{-}N]_{X_phloem})}{R_{phloem_leaf_X}} \quad (12.1)$$

in which $R_{phloem_leaf_X}$ is transport resistance between leaf phloem and X phloem (Supplementary Table 1).

Loading and unloading: Rate of substrate *s* loading and unloading at each source or sink organ X ($v_{X_s_l}$ and $v_{X_s_ul}$) were modeled with a simple equation which describes

metabolites transport across membranes, similar to that in Wang, et al. [35]:

$$v_{\mathrm{X_s_l}} = v_{\mathrm{m_X_s_l}} \cdot \frac{[\mathrm{s}]_{\mathrm{X}} - \dfrac{[\mathrm{s}]_{\mathrm{X}}}{K_{\mathrm{e_X_s_l}}}}{K_{\mathrm{m_X_s_l}} + [\mathrm{s}]_{\mathrm{X}}} \tag{13.1}$$

$$v_{\mathrm{X_s_ul}} = v_{\mathrm{m_X_s_ul}} \cdot \frac{[\mathrm{s}]_{\mathrm{tube}} - \dfrac{[\mathrm{s}]_{\mathrm{X}}}{K_{\mathrm{e_X_s_ul}}}}{K_{\mathrm{m_X_s_ul}} + [\mathrm{s}]_{\mathrm{tube}}} \tag{13.2}$$

in which $K_{\mathrm{m_X_s_l}}$ and $K_{\mathrm{m_X_s_ul}}$ are Michaelis-constants; $v_{\mathrm{m_X_s_l}}$ is maximal loading rate and $v_{\mathrm{m_X_s_ul}}$ is maximal unloading rate of substrate *s* at organ X; $[\mathrm{s}]_{\mathrm{X}}$ and $[\mathrm{s}]_{\mathrm{tube}}$ are the concentrations of substrate *s* in organ X and in xylem or phloem tube, respectively. These loading and unloading processes include root-to-shoot I-N and O-N loading (to xylem), shoot-to-root sucrose and O-N unloading (from phloem) at root; photosynthetic sucrose and O-N loading (to phloem), I-N and O-N unloading (from xylem) at leaf; sucrose and O-N unloading (from phloem) at grain; and xylem-to-phloem O-N transfer (see Figure 1, process 13).

Phloem-stem diffusion: As a simplification, stem was set to locate around leaf phloem only. Substrates (sucrose and O-N in this model) difffusion rate ($v_{\mathrm{phloem_stem_s_d}}$) between leaf phloem and stem were determined by their diffusion property:

$$v_{\mathrm{phloem_SSP_s_d}} = \frac{[\mathrm{s}]_{\mathrm{phloem}} - [\mathrm{s}]_{\mathrm{SSP}}}{\mathrm{R}_{\mathrm{_phloem_SSP_s}}} \tag{14.1}$$

in which $[\mathrm{s}]_{\mathrm{phloem}}$ and $[\mathrm{s}]_{\mathrm{stem}}$ are substrate *s* concentration in leaf phloem and stem, respectively; $\mathrm{R}_{\mathrm{_phloem_stem_s}}$ is transfer resistance of substrate *s* (Supplementary Table 1).

Respiration

Plant dark respiration rate was calculated for each organ ($R_{\mathrm{d_root}}$, $R_{\mathrm{d_leaf}}$, $R_{\mathrm{d_grain}}$, $R_{\mathrm{d_stem}}$), following the concept proposed by Cannell and Thornley [129]:

$$\begin{aligned} R_{\mathrm{d_root}} = [&\eta_{\mathrm{l}} \cdot (v_{\mathrm{root_IN_l}} + v_{\mathrm{root_ON_l}} + v_{\mathrm{root_ON_ul}} + v_{\mathrm{root_Suc_ul}}) + \eta_{\mathrm{N_upt}} \cdot v_{\mathrm{root_N_upt}} \\ &+ \eta_{\mathrm{N_ass}} \cdot v_{\mathrm{root_N_ass}} + \eta_{\mathrm{grow}} \cdot v_{\mathrm{root_grow}}] \cdot \mathrm{RW} + \gamma_{\mathrm{root_residual}} \cdot V_{\mathrm{root_aq}} \end{aligned} \tag{15.1}$$

$$\begin{aligned} R_{\mathrm{d_leaf}} = [&\eta_{\mathrm{l}} \cdot (v_{\mathrm{leaf_ON_l}} + v_{\mathrm{leaf_Suc_l}} + v_{\mathrm{leaf_IN_ul}} + v_{\mathrm{leaf_ON_ul}}) + \eta_{\mathrm{store}} \cdot v_{\mathrm{leaf_Star_deg}} \\ &+ \eta_{\mathrm{Pro_syn}} \cdot v_{\mathrm{leaf_Pro_syn}} + \eta_{\mathrm{Pro_deg}} \cdot v_{\mathrm{leaf_Pro_deg}}] \cdot \mathrm{LA} + \gamma_{\mathrm{residual}} \cdot V_{\mathrm{leaf_aq}} \end{aligned} \tag{15.2}$$

$$R_{\text{d_grain}} = [\eta_{\text{ul}} \cdot (v_{\text{grain_ON_ul}} + v_{\text{grain_Suc_ul}}) + \eta_{\text{grow}} \cdot v_{\text{grain_grow}}] \cdot S_{\text{grain}} + (\eta_{\text{store}} \cdot v_{\text{grain_Star_syn}} + \eta_{\text{Pro_syn}} \cdot v_{\text{grain_Pro_syn}}) \cdot V_{\text{grain_aq}} + \gamma_{\text{residual}} \cdot V_{\text{grain}} \quad (15.3)$$

$$R_{\text{d_stem}} = [\eta_{\text{store}} \cdot (v_{\text{stem_Star_deg}} + v_{\text{stem_Star_syn}}) + \eta_{\text{Pro_syn}} \cdot v_{\text{stem_Pro_syn}} + \eta_{\text{Pro_deg}} \cdot v_{\text{stem_Pro_deg}} + \gamma_{\text{residual}}] \cdot V_{\text{stem_aq}} \quad (15.4)$$

in which η_{l}, η_{ul}, $\eta_{\text{N_upt}}$, $\eta_{\text{N_ass}}$, η_{grow}, η_{store}, $\eta_{\text{Pro_deg}}$ and $\eta_{\text{Pro_syn}}$ are respiration coefficients of loading, unloading, soil I-N uptake, N assimilation, growth, starch degdaration or synthesis, protein degradation and protein synthesis processes, respectively; $v_{\text{X_IN_l}}$ and $v_{\text{X_ON_l}}$ and $v_{\text{X_Suc_l}}$, $v_{\text{X_IN_ul}}$ and $v_{\text{X_ON_ul}}$ and $v_{\text{X_Suc_ul}}$, $v_{\text{X_N_upt}}$, $v_{\text{X_N_ass}}$, $v_{\text{X_grow}}$, $v_{\text{X_Star_deg}}$ and $v_{\text{X_Star_syn}}$, $v_{\text{X_Pro_deg}}$ and $v_{\text{X_Pro_syn}}$ are the corresponding reaction rates in organ X; $V_{\text{root_aq}}$, $V_{\text{leaf_aq}}$, $V_{\text{grain_aq}}$ and $V_{\text{stem_aq}}$ are the aqueous space volume of root, leaf, grain and stem, respectively; γ_{residual} is the residual respiration (respiration for other processes) coefficient for leaf, stem and grain; $\gamma_{\text{root_residual}}$ is the residual respiration coefficient for root, which is twice larger than γ_{residual} as a compensation for potential root exudation that is not explicitly represented in the model (Supplementary Table 1).

Model parameterization

The maximal velocities (v_{max}) for processes modeled in WACNI were derived from a vast amount of genetic, molecular, biochemical and plant physiological research in rice; while most of the apparent Michaelis-constants (K_{m}) and equilibrium constants (K_{e}) were estimated based on initial metabolite concentrations in each organ. A detailed description of parameters, their values, and the comprehensive parameterization procedure used to derive or estimate their values are given in Supplementary Table 1.

Model validation on multiple datasets

Simulating typical plant physiological changes during rice grain filling period (Figure 2a-f)

WACNI was firstly validated by comparing the relative changes of physiological traits in different organs during the grain filling period between model predictions with default parameter settings and experimental data obtained from literatures under normal conditions (Figure 2a-f). Specifically, data of root weight dynamic change (Figure 2a) were extracted from *Table 2* in Tang, et al. [50], and the average values of seven combinations of two-line hybrid rice were used; data of leaf area dynamic change (Figure 2b) were extracted from *Figure 1(d)* in Haque, et al. [51], and the average values of three hybrid and inbred varieties in 2008-09 were used; data of canopy photosynthesis (Figure 2c) were extracted from *Fig. b* in Zhao, et al. [52], and values of treatment F3 were used; data of grain volume (Figure 2d) and grain dry weight (Figure 2e) were extracted from *Fig. 1c* and *Fig. 2c* in Yang, et al. [53], respectively, and values of spikelets of cultivar Yangdao 4 that flowered on the fourth day were used; data of stem non-structural carbohydrate (Figure 2f) were extracted from *Fig. 4B* in Yang, et al. [54], and the average values of normal nitrogen with well-watered and water deficit stressed treatments of cultivar Yangdao 4 were used. All the extracted experimental data are tabulated in Supplementary Datasets 2.

Simulating plant carbon and nitrogen fluxes during rice grain filling period (Figure 2g)

Specifically, total carbon content in a plant at flowering (PTC0) was calculated as:

$$\begin{aligned}\mathrm{PTC0}=&\mathrm{RW0}+\mathrm{SSW0}+\mathrm{LA0}/\mathrm{SLA}+\mathrm{SStar0}+\mathrm{SPro0}+\mathrm{LPro0}+\\&\mathrm{RV0}\cdot(c_{\mathrm{root_ON}}+c_{\mathrm{root_IN}}+c_{\mathrm{root_Suc}})+\mathrm{SV0}\cdot(c_{\mathrm{stem_ON}}+c_{\mathrm{stem_Suc}})+\\&\mathrm{LV0}\cdot(c_{\mathrm{leaf_ON}}+c_{\mathrm{leaf_IN}}+c_{\mathrm{leaf_Suc}})+\mathrm{PV0}\cdot(c_{\mathrm{phloem_ON}}+c_{\mathrm{phloem_Suc}})+\\&\mathrm{XV0}\cdot(c_{\mathrm{xylem_ON}}+c_{\mathrm{xylem_IN}})\end{aligned}$$

in which RW0, SSW0, LA0, SLA, SStar0, SPro0 and LPro0 are root weight, stem structural weight, leaf area, specific leaf area, stem stored starch weight, stem stored protein weight and leaf protein weight at flowering, respectively; RV0, SV0, LV0, PV0 and XV0 are root volume, stem volume, leaf volume, phloem volume and xylem volume, respectively; $c_{\mathrm{x_y}}$ are concentration of metabolite *y* in organ *x*.

Total nitrogen content in a plant at flowering (PTN0) was calculated as:

$$\begin{aligned}\mathrm{PTN0}=&\mathrm{RW0}\cdot c_{\mathrm{root_strucN}}+\mathrm{SSW0}\cdot c_{\mathrm{stem_strucN}}+\mathrm{LA0}/\mathrm{SLA}\cdot c_{\mathrm{leaf_strucN}}+\\&\mathrm{RV0}\cdot(c_{\mathrm{root_ON}}+c_{\mathrm{root_IN}})+\mathrm{SV0}\cdot c_{\mathrm{stem_ON}}+\mathrm{LV0}\cdot(c_{\mathrm{leaf_ON}}+c_{\mathrm{leaf_IN}})+\\&\mathrm{PV0}\cdot c_{\mathrm{phloem_ON}}+\mathrm{XV0}\cdot(c_{\mathrm{xylem_ON}}+c_{\mathrm{xylem_IN}})+\\&\mathrm{SPro0}+\mathrm{LPro0}\end{aligned}$$

For default model parameters, PTN0=49 mmol/plant.

For the carbon budget, we calculated several types of carbon fluxes. They are:

- leaf respiration to total photosynthetically fixed carbon = 504/2328*100% = 21.6%;
- entire plant respiration to total photosynthetically fixed carbon = [420+504+84+204]/2328*100% = 52.1%;
- contribution of photosynthesis-derived carbon to grain filling = 1764/[1764+240]*100% = 88.0%;
- contribution of stem non-structural carbohydrate storage to grain filling = 240/[1764+240]*100% = 12.0%;
- ratio between stem weight loss during grain filling to grain yield at harvest = [240+84]/[1608-420]*100% = 27.3%;
- ratio of carbohydrates partitioning to root from flowering to harvest = 396/[396+1608]*100% = 19.8%;
- ratio of carbohydrates partitioning to ear from flowering to harvest = 100% - 19.8% = 80.2%.

For nitrogen budget, we calculated several types of nitrogen fluxes. They are:

- ratio of nitrogen assimilation in root = 7.8/[7.8+12.4]*100% = 38.6%;
- ratio of nitrogen assimilation in leaf = 100% - 38.6% = 61.4%;

- ratio of root nitrogen uptake after flowering to whole season nitrogen uptake = 20/[20+49]*100% = 29.0%;
- nitrogen harvest index = 43.3/[20+49]*100% = 62.8%.

Simulating effects of different nitrogen fertilizer application rates on rice grain filling (Figure 3a-l)

To examine effects of different nitrogen fertilizer application rates on rice grain filling, experimental data were collected from Zhao, et al. [57] (Supplementary Datasets 2). The authors reported four nitrogen topdressing treatments during the ear development period, i.e., no nitrogen was applied; low level (0.6 g nitrogen/pot), medium level (1.2 g nitrogen/pot), and high level (1.8 g nitrogen/pot) nitrogen were applied. In simulation, soil nitrogen concentrations were set to be 20%, 50%, 100% and 150% of the default value for the four nitrogen treatments, respectively, with the assumption that there was still 20% of nitrogen in soil when no nitrogen was applied. According to *Table 1* in Zhao, et al. [57], ratio of leaf dry matter and grains dry weight per plant among the four nitrogen treatments at 7 days after anthesis were 0.60 : 0.90 : 1.00 : 1.23, and 0.43 : 0.75 : 1.00 : 1.18, respectively. Therefore, we set ratio of tiller number between these groups as that of leaf dry matter, i.e., 0.60 : 0.90 : 1.00 : 1.23, and set ratio of grain number per ear between these groups by dividing grains dry weight by tiller number, i.e., 0.43/0.60 : 0.75/0.90 : 1.00 : 1.18/1.23. According to *Table 2* of Zhao, et al. [57], ratio of leaf protein amino acids per plant between the four nitrogen treatments at 7 days after anthesis were 0.40 : 0.75 : 1.00 : 1.21. Therefore, we set ratio of leaf protein concentration between groups by dividing leaf protein amino acids by leaf dry matter, i.e., 0.40/0.60 : 0.75/0.90 : 1.00 : 1.21/1.23. We further set the same ratio of stem protein concentration between groups as that of leaf. In addition, tiller number per plant for the medium nitrogen treatment was set to 11.

For the sake of comparing physiological traits during the grain filling period between model simulation and experimental data, grain nitrogen concentration data were

extracted from *Table 2* in Zhao, et al. [57], and values of total amino acids were used; leaf nitrogen concentration data were calculated by dividing amount of leaf total amino acids by leaf dry matter from *Table 1* and *Table 2* in Zhao, et al. [57], grain dry weight data were extracted from *Table 1* in Zhao, et al. [57]. For both model simulation and experimental data, values of leaf nitrogen concentration, grain nitrogen concentration at 7 days after flowering and grain dry weight at harvest of the medium nitrogen treatment were used as a reference, and data at all time points and in all nitrogen treatment groups were normalized by dividing these values, respectively. Extracted experimental data are tabulated in Supplementary Datasets 2.

Simulating effects of shading and thinning on rice grain filling (Figure 3m-s)

To examine effects of different light regimes on rice grain filling, experimental data were collected from Kobata, et al. [58] (Supplementary Datasets 2). The authors reported seven different shading/thinning treatments after flowering. Firstly, control plots were grown under normal condition throughout the entire grain filling period. Concurrently, three shading treatments were applied immediately after flowering, i.e., the heavy shaded treatment using double black cloth, the moderate shaded treatment using single black cloth, and the light shaded treatment using white cloth, which reduced full sun radiation by 74.4%, 48.1% and 25.1%, respectively. The shade frames were removed 10 days later. Then, half the plots were left untouched (Figure 3n-p), while the other half were thinned to every other plant to reduce the plant density by half for the rest of the grain filling period (Figure 3q-s).

Default model parameters were used during simulation. In WACNI, incident solar light intensity during the firstly 10 days after flowering were reduced to 75%, 50% and 25% for light, medium and heavy shaded treatments, respectively; and the planting density beyond 10 days after flowering were halved for the thinning treatment groups. Experimental data of grain dry weight changes during the grain filling period for all seven treatments were extracted from *Fig. 2* in Kobata, et al. [58]. For both model

simulation and experimental data, values of grain dry weight at harvest of the 'normal condition' group were used as a reference, and data at all time points and for all treatments were normalized by dividing them, respectively. Extracted experimental data are tabulated in Supplementary Datasets 2.

Simulating interaction effects of different nitrogen fertilizer application rates and air CO_2 concentrations on rice grain filling (Figure 3t-u)

For simulating interaction effects of different nitrogen fertilizer application rates and air CO_2 concentrations on rice grain filling, experimental data were collected from Kim, et al. [59] (Supplementary Datasets 2). The authors reported six different combinations of nitrogen fertilizer application rate and air CO_2 concentration treatments. Namely, nitrogen was supplied as ammonium sulphate at three application rates: 4 g m^{-2} (low; 'LN'), 8-9 g m^{-2} (medium; 'MN') and 12-15 g m^{-2} (high; 'HN'), respectively; air CO_2 concentration was controlled at two levels: ambient level of around 390 μmol mol^{-1}, free-air CO_2 enrichment of 230-365 μmol mol^{-1} higher than that under ambient level ('FACE'). Correspondingly, in the simulation, we set the soil nitrogen concentrations to be 50%, 100% and 150% of the default value for 'LN', 'MN' and 'HN' treatments, respectively; the air CO_2 concentrations were set to 390 and 690 μmol mol^{-1} for ambient and 'FACE' treatments, respectively.

According to *Table 1* in Kim, et al. [59], it was known that ratio of plant total nitrogen, plant root dry matter and plant total dry matter between 'LN', 'MN', 'HN', 'LN+FACE', 'MN+FACE' and 'HN+FACE' groups at ear initiation were 0.83 : 1.00 : 1.25 : 0.85 : 1.15 : 1.53, 1.00 : 1.00 : 1.03 : 1.18 : 1.46 : 1.35 and 0.87 : 1.00 : 1.06 : 1.21 : 1.45 : 1.51, respectively. Therefore, ratio of root weight between these groups at flowering was set as that of plant root dry matter measured at ear initiation; ratio of leaf area and pre-flowering stem stored starch at flowering was set to be the same as that of measured plant total dry matter at ear initiation; and ratio of leaf protein concentration and pre-flowering stem stored protein at flowering was set by dividing plant total nitrogen by

plant total dry matter, i.e., 0.83/0.87 : 1.00 : 1.25/1.06 : 0.85/1.21 : 1.15/1.45 : 1.53/1.51.

According to *Table 2* in Kim, et al. [59], it was known that ratio of ear number, fertile spikelets and individual grain mass between 'LN', 'MN', 'HN', 'LN+FACE', 'MN+FACE' and 'HN+FACE' groups at harvest were 0.87 : 1.00 : 1.07 : 0.89 : 1.09 : 1.15, 0.83 : 1.00 : 1.13 : 0.85 : 1.09 : 1.30, and 1.07 : 1.00 : 0.98 : 1.09 : 1.04 : 0.93, respectively. Therefore, ratio of tiller number and grain size between these groups was set as that of ear number and individual grain mass measured at harvest, respectively; ratio of grain number per ear between these groups was set by dividing fertile spikelets by tiller number, i.e., 0.83/0.87 : 1.00 : 1.13/1.07 : 0.85/0.89 : 1.09/1.09 : 1.30/1.15. Ratio of leaf nitrogen concentration at flowering was set by dividing plant nitrogen uptake by plant total dry matter at panicle initiation, which was 0.95 : 1.00 : 1.18 : 0.70 : 0.79 : 1.01. In addition, grain number per ear was set to 145 for the 'MN' group.

During comparison of model prediction and experimental data, grain yield at harvest was extracted from *Table 2* in Kim, et al. [59], root nitrogen uptake throughout the grain filling period was approximated by the difference of plant total nitrogen at harvest and plant total nitrogen at ear initiation from *Table 1* in Kim, et al. [59]. We simulated two scenarios, one was using adjusted parameters as above mentioned, with other parameters using the default values (the 'Simulation' group in Figure 3t, u); the other one was with a further assumption that maximal root nitrogen uptake rate under 'FACE' was reduced by 36% compared to that under ambient condition (the 'Simulation (v_{m_Nupt}=64% under FACE)' group in Figure 3t, u). For both model simulation and experimental data, values of grain yield and root nitrogen uptake in the 'MN' group were used as a reference, and data at all time points and for all treatments were normalized by dividing them, respectively. Extracted experimental data are tabulated in Supplementary Datasets 2.

Simulating effects of genetic manipulation of leaf senescence rate on rice grain filling (Figure 4a-c)

To examine effects of genetic manipulation of leaf senescence rate on rice grain filling, experimental data were collected from Liang, et al. [61] (Supplementary Datasets 2). The authors reported a gain-of-function mutant prematurely senile 1 (*ps1-D*) that demonstrated significant premature leaf senescence. Further genetic study shows that *PS1* encodes a plant-specific NAC transcription activator, *OsNAP*, overexpression of which significantly promoted senescence, whereas knockdown of which would delay leaf senescence. Default model parameters were used for simulating wild type plants ('WT'), except that the $v_{\mathrm{m_leaf_Pro_deg}}$ was set to 50% of the default value. According to *Fig. 1C* in Liang, et al. [61], expression of chlorophyll degradation and leaf senescence process related genes in '*ps1-D* mutant' increased to 3-5 folds to that of 'WT'; and according to *Fig. 4B-C* in Liang, et al. [61], *OsNAP* gene expression level in leaf of '*OsNAP* RNAi' decreased to 0.2-0.3 fold, while ABA content increased to 1.4-1.9 folds to that of 'WT'. Therefore, we set $v_{\mathrm{m_leaf_Pro_deg}}$ of '*ps1-D* mutant' and '*OsNAP* RNAi' to be 0.5-fold and 4-folds of 'WT', respectively.

According to *Table S4* in Liang, et al. [61], ratio of dry weight of vegetative organs among 'WT', '*ps1-D* mutant' and '*OsNAP* RNAi' groups was 1 : 0.74 : 1.11. Therefore, ratio of plant size between these groups, including leaf area, root weight, stem stored starch/protein and grain number per ear, were set the same as that for dry weight of vegetative organs, i.e., 1 : 0.74 : 1.11.

To enable comparison between model predictions and experimental data, we extracted leaf chrolophyll content dynamic changes of 'WT' and '*ps1-D* mutant'during the grain filling period from *Fig. 1B* in Liang, et al. [61], which was used to represent relative change of leaf nitrogen concentration. Grain yield and grain nitrogen concentration at harvest were extracted from *Fig. 4F* and *Fig. 5B* in Liang, et al. [61], respectively. For both model simulation and experimental data, values of leaf nitrogen concentration at flowering, and grain yield and grain nitrogen concentration at harvest of 'WT' were used as a reference, i.e., data at all time points and for other plants were normalized by dividing them, respectively. Extracted experimental data are tabulated in

Supplementary Datasets 2.

Simulating effects of genetic manipulation of grain sucrose unloading capacity on rice grain filling (Figure 4d)

To examine effects of genetic manipulation of grain sucrose unloading capacity on rice grain filling, experimental data were collected from Wang, et al. [62] (Supplementary Datasets 2). The authors reported a loss-of-function mutant grain incomplete filling 1 ('*gif1* mutant') that showed slower grain-filling rate than wild-type rice ('WT'). Further genetic study shows that *GIF1* encodes a cell-wall invertase, which is responsible for sucrose unloading into grain, particularly during early grain-filling. As shown in Figure 1g of Wang, et al. [62], the grain filling duration was as short as less than 30 days, we halved the leaf area, root weight and stem stored starch/protein from default values, set grain number per ear to 90, and set the maximal rate of sucrose unloading to grain as 200% of the default value for 'WT'.

According to *Figure 1h-j* in Wang, et al. [62], sugar content at 5 days after pollination in '*gif1* mutant' decreased to 0.4-0.7 fold to that of 'WT'. Therefore, the maximal grain sucrose unloading rate of '*gif1* mutant' was set to be 0.5-fold of 'WT'; the maximal grain sucrose unloading rate of plants overexpressing *GIF1* from its native promoter ('*GIF1* OE') was set to be 2-fold of 'WT'.

According to *Figure 1g* and *Figure 4b* in Wang, et al. [62], ratio of grain dry weight at harvest between 'WT', '*gif1* mutant' and '*GIF1* OE' groups was 1 : 0.76 : 1.11. Therefore, ratio of grain size between these groups was set to be the same as that for measured grain dry weight at harvest, i.e., 1 : 0.76 : 1.11. Extracted experimental data are tabulated in Supplementary Datasets 2.

For both model simulation and experimental data, grain dry weights at harvest of 'WT' were used as a reference, i.e., data at all time points and for other plants were normalized by dividing them, respectively.

To test the effects of changing grain sucrose unloading capacity on plant physiological changes during the grain filling period for 'source limited' plants (with default model parameter settings except that the grain number per ear is set to 190), we further simulated grain dry weight, leaf nitroge concentration, canopy photosynthesis, root dry weight and root nitrogen uptake throughout the grain filling period for plants with maximal grain sucrose unloading rates of 200%, 100% and 50% to that of the default value.

Simulating effects of genetic manipulation of grain starch synthesis capacity on rice grain filling (Figure 4e)

To examine effects of genetic manipulation of grain starch synthesis capacity on rice grain filling, experimental data were collected from Smidansky, et al. [63] (Supplementary Datasets 2). The authors reported that transforming rice with a modified maize AGPase large subunit sequence (*Sh2r6hs*) in an endosperm-specific manner could specifically enhance capacity for starch synthesis in endosperm. According to *Table 4* in Smidansky, et al. [63], the grain number per ear was only 90 for negative homozygotes of *Sh2r6hs* transgene ('WT') plants. Therefore, the leaf area, root weight and stem stored starch/protein were halved from default values, and grain number per ear was set to 90 for 'WT' plants. According to *Table 4* in Smidansky, et al. [63], ratio of grain number per ear and tiller number between 'WT' and *Sh2r6hs* transgene groups were 1 : 1.13 and 1 : 1.05, respectively. Ratio of grain size between two groups was set to be the same as that for grain weight, i.e., 1: 1.02. Ratio of leaf area, root weight, stem structural weight, stem starch storage and stem protein storage was set by dividing total plant weight by tiller number, i.e., 1 : 1.22/1.05. According to *Table 2* in Smidansky, et al. [63], the measured AGPase activity was 9-52% higher in *Sh2r6hs* transgenic grains than in untransformed grains between 10-20 days after anthesis. Therefore, the maximal grain starch synthesis rate $v_{\mathrm{m_grain_Star_syn}}$ of *Sh2r6hs* transgenic plants was set to be 1.5-fold of 'WT'.

In total three scenarios were simulated, the first one was using adjusted plant size and $v_{m_grain_Star_syn}$ as above mentioned, with other parameters using the default values (the grey bars in Figure 4e); the second one was using only adjusted plant size with unchanged $v_{m_grain_Star_syn}$ (the black bars Figure 4e); the third one was using only adjusted $v_{m_grain_Star_syn}$ with unchanged plant size (the white bars Figure 4e).

To enable comparison between model predictions and experimental data, we extracted grain yield, grain nitrogen concentration and harvest index at harvest of positive homozygotes and negative homozygotes of *Sh2r6hs* transgenic plants from *Table 4* in Smidansky, et al. [63]. For both model simulation and experimental data, grain yield, grain nitrogen concentration and harvest index at harvest of negative homozygotes of *Sh2r6hs* transgenic plants were used as a reference, i.e., data at all time points and for other plants were normalized by dividing them, respectively. Extracted experimental data are tabulated in Supplementary Datasets 2.

Sensitivity analysis of model parameters

To conduct parameter perturbations, 26 model parameters controlling capacities of biochemical processes (v_{max_*}) and two phloem resistance parameters ($R_{_phloem_leaf_root}$ and $R_{_phloem_leaf_grain}$) were perturbed within [0.1, 10] folds to their default values individually. Grain number per ear was set to 190 for each group to allow sufficient sink capacity. Grain yield and values of other seven agronomic traits were calculated for each simulation, i.e., whole grain-filling season total canopy photosynthesis, whole grain-filling season total root nitrogen uptake, active grain filling duration, grain nitrogen concentration at harvest, average grain filling rate from flowering to harvest, dry matter harvest index and nitrogen harvest index. The active grain filling duration (GFD) was determined as the time interval between flowering day and the day when total grain dry weight ($TGDW_1$) reaches 95% of its maximal value (at the end of the simulation), and average grain filling rate (GFR) was calculated as:

$$GFR=\frac{TGDW_1}{GFD}$$

Identification of optimal parameter combinations to maximize grain yield using a genetic algorithm

A genetic algorithm was used to identify the optimal value combinations of parameters to maximize grain yield. In brief, this algorithm mimics the process of natural biological evolution. the above mentioned 28 molecular biochemical/biophysical parameters, together with partitioning of initial mass between three organs at flowering, i.e., root weight, leaf area and grain number, were perturbed independently by randomly multiplying a scaling coefficient ranging from 0.5 to 2. Grain yield was used as the selection pressure in the algorithm.

To avoid a local optimum at the end of the evolution, five independent evolutionary populations under normal condition (ambient CO_2 concentration is 400 μbar; soil I-N concentration is 0.14 mol m^{-3}; grain-filling season is 50 days; see light intensity, air temperature and humidity information in Supplementary Figure 14) were constructed. Each of the evolutionary populations has 100*100 individuals, i.e., 100 generations with 100 individuals in each generation. As mentioned above, each parameter was restricted to vary between 0.5 to 2-fold of its default value. For the sake of comparison between lines, for each individual in the virtual population, we restrict the total plant equivalent carbon and nitrogen at flowering to be the same. Specifically, for total plant equivalent carbon balance, we have:

$$\frac{\Delta SStar0}{\eta_{store}} = -\frac{\Delta RW0+\Delta LA0 / SLA+\Delta GN0 \cdot HW}{\eta_{grow}}$$

in which Cstar0, RW0, LA0 and GN0 are stem stored starch weight, root weight, leaf area and grain number at flowering, respectively; η_{grow} is growth efficiency, i.e., the ratio of biomass production to the sucrose consumption (g g^{-1}); η_{store} is storage efficiency, i.e., the ratio of carbon fixed in starch to the total amount of carbon used by sucrose [mol C (mol C) $^{-1}$]; SLA is specific leaf area; HW is husk weight per spikelet.

Amount of total nitrogen in leaf is a constant:

$$\Delta LP0 = -\Delta LA0 / SLA \cdot c_{leaf_strucN} - \Delta LV0 \cdot (c_{leaf_ON} + c_{leaf_IN})$$

in which LP0 and LV0 are total leaf protein and leaf volume at flowering, respectively; c_{leaf_ON} and c_{leaf_IN} are concentrations of leaf organic nitrogen and inorganic nitrogen, respectively; c_{leaf_strucN} is nitrogen concentration for leaf structural matter.

Amount of total nitrogen in root, stem and grain is a constant:

$$\Delta SPro0 = -(\Delta RW0 \cdot c_{root_strucN} + \Delta RV0 \cdot (c_{root_ON} + c_{root_IN}) + \Delta GN0 \cdot HW \cdot c_{husk_strucN})$$

in which SPro0 and RV0 are stem stored protein and total root volume at flowering, respectively; c_{root_ON} and c_{root_IN} are concentrations of root organic nitrogen and inorganic nitrogen, respectively; c_{root_strucN} and c_{husk_strucN} are nitrogen concentration for root and husk structural matter, respectively.

Data and software availability

Experimental data extracted from literature that used in model parameterization and model-data comparison were given in Supplementary Datasets 2.

Source code is free for use for academic and non-commercial applications upon request.

References

1 Ray, D. K., Mueller, N. D., West, P. C. & Foley, J. A. Yield trends are insufficient to double global crop production by 2050. *PLoS One* **8**, e66428 (2013).

2 Long, S. P., Marshall-Colon, A. & Zhu, X.-G. Meeting the global food demand of the future by engineering crop photosynthesis and yield potential. *Cell* **161**, 56-66 (2015).

3 Zhao, C. *et al.* Temperature increase reduces global yields of major crops in four independent estimates. *Proc Natl Acad Sci USA* **114**, 9326-9331, doi:10.1073/pnas.1701762114 (2017).

4 Bailey-Serres, J., Parker, J. E., Ainsworth, E. A., Oldroyd, G. E. D. & Schroeder, J. I. Genetic strategies for improving crop yields. *Nature* **575**, 109-118, doi:10.1038/s41586-019-1679-0 (2019).

5 Peleman, J. D. & van der Voort, J. R. Breeding by design. *Trends Plant Sci* **8**, 330-334, doi:10.1016/S1360-1385(03)00134-1 (2003).

6 Wang, Y. *et al.* Simultaneous editing of three homoeoalleles in hexaploid bread wheat confers heritable resistance to powdery mildew. *Nat Biotechnol* **32**, 947-951 (2014).

7 Mickelbart, M. V., Hasegawa, P. M. & Bailey-Serres, J. Genetic mechanisms of abiotic stress tolerance that translate to crop yield stability. *Nature Reviews. Genetics* **16**, 237 (2015).
8 Qian, Q., Guo, L. B., Smith, S. M. & Li, J. Y. Breeding high-yield superior quality hybrid super rice by rational design. *Natl Sci Rev* **3**, 283-294, doi:10.1093/nsr/nww006 (2016).
9 Zeng, D. L. *et al.* Rational design of high-yield and superior-quality rice. *Nat Plants* **3**, 17031, doi:10.1038/Nplants.2017.31 (2017).
10 Hartung, F. & Schiemann, J. Precise plant breeding using new genome editing techniques: opportunities, safety and regulation in the EU. *The Plant Journal* **78**, 742-752 (2014).
11 Araus, J. L. & Cairns, J. E. Field high-throughput phenotyping: the new crop breeding frontier. *Trends Plant Sci* **19**, 52-61 (2014).
12 Wallace, J. G., Rodgers-Melnick, E. & Buckler, E. S. On the road to breeding 4.0: unraveling the good, the bad, and the boring of crop quantitative genomics. *Annual Review of Genetics* **52**, 421-444, doi:10.1146/annurev-genet-120116-024846 (2018).
13 Watt, M. *et al.* Phenotyping: new windows into the plant for breeders. *Annu Rev Plant Biol* **71**, 689-712, doi:10.1146/annurev-arplant-042916-041124 (2020).
14 Chang, T.-G., Chang, S., Song, Q.-F., Perveen, S. & Zhu, X.-G. Systems models, phenomics and genomics: three pillars for developing high-yielding photosynthetically efficient crops. *In Silico Plants* **1**, doi:10.1093/insilicoplants/diy003 (2019).
15 White, A. C., Rogers, A., Rees, M. & Osborne, C. P. How can we make plants grow faster? A source–sink perspective on growth rate. *J Exp Bot* **67**, 31-45, doi:10.1093/jxb/erv447 (2015).
16 Xing, Y. & Zhang, Q. Genetic and molecular bases of rice yield. *Annu Rev Plant Biol* **61**, 421-442 (2010).
17 Wang, Y. & Li, J. Molecular basis of plant architecture. *Annu Rev Plant Biol* **59**, 253-279 (2008).
18 Li, Z., Pinson, S. R. M., Stansel, J. W. & Paterson, A. H. Genetic dissection of the source-sink relationship affecting fecundity and yield in rice (shape *Oryza sativa* L.). *Mol Breed* **4**, 419-426 (1998).
19 Donald, C. M. The breeding of crop ideotypes. *Euphytica* **17**, 385-403 (1968).
20 Chen, W., Xu, Z., Zhang, W., Zhang, L. & Yang, S. Creation of new plant type and breeding rice for super high yield. *Acta Agronomica Sinica* **27**, 665-672 (2000).
21 Peng, S., Khush, G. S., Virk, P., Tang, Q. & Zou, Y. Progress in ideotype breeding to increase rice yield potential. *Field Crops Res* **108**, 32-38 (2008).
22 Yuan, L. Progress in super-hybrid rice breeding. *Crop J* **5**, 100-102 (2017).
23 Jiao, Y. Q. *et al.* Regulation of *OsSPL14* by OsmiR156 defines ideal plant architecture in rice. *Nat Genet* **42**, 541-544, doi:10.1038/ng.591 (2010).
24 Song, Q. F., Zhang, G. L. & Zhu, X. G. Optimal crop canopy architecture to maximise canopy photosynthetic CO_2 uptake under elevated CO_2 - a theoretical study using a mechanistic model of canopy photosynthesis. *Funct Plant Biol* **40**, 109-124, doi:10.1071/FP12056 (2013).
25 Zhang, L. *et al.* A natural tandem array alleviates epigenetic repression of IPA1 and leads to superior yielding rice. *Nat Commun* **8**, doi:10.1038/ncomms14789 (2017) (2017).
26 Pan, Q. *et al.* The genetic basis of plant architecture in 10 maize recombinant inbred line populations. *Plant Physiol* **175**, 858-873, doi:10.1104/pp.17.00709 (2017).
27 Long, S. P., Zhu, X. G., Naidu, S. L. & Ort, D. R. Can improvement in photosynthesis increase crop yields? *Plant Cell Environ* **29**, 315-330, doi:10.1111/j.1365-3040.2005.01493.x (2006).
28 Simkin, A. J., López-Calcagno, P. E. & Raines, C. A. Feeding the world: improving photosynthetic efficiency for sustainable crop production. *J Exp Bot* **70**, 1119–1140, doi:10.1093/jxb/ery445 (2019).
29 Sonnewald, U. *et al.* The Cassava Source–Sink project: opportunities and challenges for crop improvement by metabolic engineering. *The Plant Journal* **n/a**, doi:10.1111/tpj.14865 (2020).
30 Chang, T.-G. & Zhu, X.-G. Source-sink interaction: a century old concept under the light of modern molecular systems biology. *J Exp Bot* **68**, 4417-4431, doi:10.1093/jxb/erx002 (2017).
31 Fernie, A. R. *et al.* Synchronization of developmental, molecular and metabolic aspects of source-sink interactions. *Nat Plants* **6**, 55-66, doi:10.1038/s41477-020-0590-x (2020).
32 Marshall-Colon, A. *et al.* Crops *in silico*: generating virtual crops using an integrative and multi-scale modeling platform. *Front Plant Sci* **8** (2017).
33 Hammer, G., Messina, C., Wu, A. & Cooper, M. Biological reality and parsimony in crop models—why we need both in crop improvement! *In Silico Plants* **1**, doi:10.1093/insilicoplants/diz010 (2019).

34 Zhu, X. G., Wang, Y., Ort, D. R. & Long, S. P. e‐photosynthesis: a comprehensive dynamic mechanistic model of C_3 photosynthesis: from light capture to sucrose synthesis. *Plant Cell Environ* **36**, 1711-1727 (2013).
35 Wang, Y., Long, S. P. & Zhu, X.-G. Elements required for an efficient NADP-malic enzyme type C_4 photosynthesis. *Plant Physiol* **164**, 2231-2246 (2014).
36 Minchin, P. E. H. & Lacointe, A. New understanding on phloem physiology and possible consequences for modelling long-distance carbon transport. *New Phytol* **166**, 771-779, doi:10.1111/j.1469-8137.2005.01323.x (2005).
37 Valentim, F. L. *et al.* A quantitative and dynamic model of the Arabidopsis flowering time gene regulatory network. *PLoS One* **10**, e0116973 (2015).
38 Buckler, E. S. *et al.* The genetic architecture of maize flowering time. *Science* **325**, 714-718, doi:10.1126/science.1174276 (2009).
39 Lynch, J. P., Nielsen, K. L., Davis, R. D. & Jablokow, A. G. SimRoot: modelling and visualization of root systems. *Plant Soil* **188**, 139-151 (1997).
40 Kromdijk, J. *et al.* Improving photosynthesis and crop productivity by accelerating recovery from photoprotection. *Science* **354**, 857-861 (2016).
41 Zhu, X. G., Ort, D. R., Whitmarsh, J. & Long, S. P. The slow reversibility of photosystem II thermal energy dissipation on transfer from high to low light may cause large losses in carbon gain by crop canopies: a theoretical analysis. *J Exp Bot* **55**, 1167-1175 (2004).
42 South, P. F., Cavanagh, A. P., Liu, H. W. & Ort, D. R. Synthetic glycolate metabolism pathways stimulate crop growth and productivity in the field. *Science* **363**, eaat9077, doi:10.1126/science.aat9077 (2019).
43 Xin, C., Tholen, D. & Zhu, X. G. The benefits of photorespiratory bypasses: How can they work? *Plant Physiol* **167**, 574-585 (2015).
44 Wu, A., Hammer, G. L., Doherty, A., von Caemmerer, S. & Farquhar, G. D. Quantifying impacts of enhancing photosynthesis on crop yield. *Nat Plants* **5**, 380-388, doi:10.1038/s41477-019-0398-8 (2019).
45 Zhang, N. *et al.* Genome-wide association of carbon and nitrogen metabolism in the maize nested association mapping population. *Plant Physiol* **168**, 575-583, doi:10.1104/pp.15.00025 (2015).
46 Li, C. *et al.* Targeted, random mutagenesis of plant genes with dual cytosine and adenine base editors. *Nat Biotechnol*, doi:10.1038/s41587-019-0393-7 (2020).
47 Walton, R. T., Christie, K. A., Whittaker, M. N. & Kleinstiver, B. P. Unconstrained genome targeting with near-PAMless engineered CRISPR-Cas9 variants. *Science* **368**, 290-296, doi:10.1126/science.aba8853 (2020).
48 Tcherkez, G. G. B. & Ribas-Carbo, M. in *Terrestrial Photosynthesis in a Changing Environment: A Molecular, Physiological, and Ecological Approach* (eds Francesco Loreto, Hipólito Medrano, & Jaume Flexas) 1-6 (Cambridge University Press, 2012).
49 Yoshida, S. *Fundamentals of rice crop science*. (Los Banos, Philippines: International Rice Research Institute., 1981).
50 Tang, W.-B. *et al.* Root characteristics of high-yield C Liangyou rice combinations of two-line hybrid rice. *Sci Agric Sinica* **43**, 2859-2868, doi:10.3864/j.issn.0578-1752.2010.14.004 (2010).
51 Haque, M. M., Pramanik, H. R., Biswas, J. K., Iftekharuddaula, K. & Hasanuzzaman, M. Comparative performance of hybrid and elite inbred rice varieties with respect to their source-sink relationship. *The Scientific World Journal* **2015** (2015).
52 Zhao, Q., Huang, P. & Ling, Q. Relations between canopy apparent photosynthesis and store matter in stem and sheath between and yield and nitrogen regulations in rice. *Sci Agric Sinica* **34**, 304-310 (2001).
53 Yang, J., Zhang, J., Wang, Z., Liu, K. & Wang, P. Post-anthesis development of inferior and superior spikelets in rice in relation to abscisic acid and ethylene. *J Exp Bot* **57**, 149-160 (2006).
54 Yang, J., Zhang, J., Wang, Z., Zhu, Q. & Wang, W. Remobilization of carbon reserves in response to water deficit during grain filling of rice. *Field Crops Res* **71**, 47-55 (2001).
55 Ida, M., Ohsugi, R., Sasaki, H., Aoki, N. & Yamagishi, T. Contribution of nitrogen absorbed during ripening period to grain filling in a high-yielding rice variety, Takanari. *Plant Prod Sci* **12**, 176-184, doi:10.1626/pps.12.176 (2009).

56 Witt, C. *et al.* Internal nutrient efficiencies of irrigated lowland rice in tropical and subtropical Asia. *Field Crops Res* **63**, 113-138, doi:10.1016/S0378-4290(99)00031-3 (1999).
57 Zhao, Y. *et al.* Nitrogen effect on amino acid composition in leaf and grain of japonica rice during grain filling stage. *J Cereal Sci* **64**, 29-33 (2015).
58 Kobata, T., Sugawara, M. & Takatu, S. Shading during the early grain filling period does not affect potential grain dry matter increase in rice. *Agron J* **92**, 411-417 (2000).
59 Kim, H., Lieffering, M., Miura, S., Kobayashi, K. & Okada, M. Growth and nitrogen uptake of CO_2 - enriched rice under field conditions. *New Phytol* **150**, 223-229 (2001).
60 Shimono, H. & Bunce, J. A. Acclimation of nitrogen uptake capacity of rice to elevated atmospheric CO_2 concentration. *Ann Bot* **103**, 87-94, doi:10.1093/aob/mcn209 (2009).
61 Liang, C. *et al.* OsNAP connects abscisic acid and leaf senescence by fine-tuning abscisic acid biosynthesis and directly targeting senescence-associated genes in rice. *Proc Natl Acad Sci USA* **111**, 10013-10018 (2014).
62 Wang, E. *et al.* Control of rice grain-filling and yield by a gene with a potential signature of domestication. *Nat Genet* **40**, 1370-1374 (2008).
63 Smidansky, E. D., Martin, J. M., Hannah, L. C., Fischer, A. M. & Giroux, M. J. Seed yield and plant biomass increases in rice are conferred by deregulation of endosperm ADP-glucose pyrophosphorylase. *Planta* **216**, 656-664, doi:10.1007/s00425-002-0897-z (2003).
64 Ni, J. *et al.* Overexpression of sugar transporter gene *PbSWEET4* of pear causes sugar reduce and early senescence in leaves. *Gene* **743**, 144582, doi:10.1016/j.gene.2020.144582 (2020).
65 Zhou, Y. *et al.* Overexpression of *OsSWEET5* in rice causes growth retardation and precocious senescence. *PLoS One* **9**, e94210-e94210, doi:10.1371/journal.pone.0094210 (2014).
66 Smidansky, E. D. *et al.* Enhanced ADP-glucose pyrophosphorylase activity in wheat endosperm increases seed yield. *Proc Natl Acad Sci USA* **99**, 1724-1729 (2002).
67 Eom, J.-S. *et al.* Impaired function of the tonoplast-localized sucrose transporter in rice, OsSUT2, limits the transport of vacuolar reserve sucrose and affects plant growth. *Plant Physiol* **157**, 109-119 (2011).
68 Thomas, H. & Ougham, H. The stay-green trait. *J Exp Bot* **65**, 3889-3900, doi:10.1093/jxb/eru037 (2014).
69 Wang, Y. *et al.* Development of a three-dimensional ray-tracing model of sugarcane canopy photosynthesis and its application in assessing impacts of varied row spacing. *Bioenergy Res* **10**, 626-634, doi:10.1007/s12155-017-9823-x (2017).
70 Deng, J. *et al.* Models and tests of optimal density and maximal yield for crop plants. *Proc Natl Acad Sci USA* **109**, 15823-15828, doi:10.1073/pnas.1210955109 (2012).
71 Song, Q., Srinivasan, V., Long, S. P. & Zhu, X.-G. Decomposition analysis on soybean productivity increase under elevated CO_2 using 3-D canopy model reveals synergestic effects of CO_2 and light in photosynthesis. *Ann Bot*, doi:10.1093/aob/mcz163 (2019).
72 Chenu, K. *et al.* Contribution of crop models to adaptation in wheat. *Trends Plant Sci* **22**, 472-490, doi:10.1016/j.tplants.2017.02.003 (2017).
73 Tuberosa, R. Phenotyping for drought tolerance of crops in the genomics era. *Front Physiol* **3**, 347-347, doi:10.3389/fphys.2012.00347 (2012).
74 Peng, B., Guan, K., Tang, J., Ainsworth, E. A. & Zhou, W. Towards a multiscale crop modelling framework for climate change adaptation assessment. *Nat Plants* **6**, 338-348 (2020).
75 Fu, J.-D., Yan, Y.-F. & Lee, B.-W. Physiological characteristics of a functional stay-green rice "SNU-SG1" during grain-filling period. *J Crop Sci Biotechnol* **12**, 47-52, doi:10.1007/s12892-009-0078-8 (2009).
76 Braun, D. M., Wang, L. & Ruan, Y.-L. Understanding and manipulating sucrose phloem loading, unloading, metabolism, and signalling to enhance crop yield and food security. *J Exp Bot* **65**, 1713-1735, doi:10.1093/jxb/ert416 (2014).
77 Yang, J. & Zhang, J. Grain filling of cereals under soil drying. *New Phytol* **169**, 223-236 (2006).
78 Cakir, B., Tuncel, A., Hwang, S.-K. & Okita, T. W. in *Starch: Metabolism and Structure* (ed Yasunori Nakamura) 371-395 (Springer Japan, 2015).
79 Yu, S.-M., Lo, S.-F. & Ho, T.-H. D. Source–sink communication: regulated by hormone, nutrient, and stress cross-signaling. *Trends Plant Sci* **20**, 844-857, doi:10.1016/j.tplants.2015.10.009 (2015).

80 Postma, J. A. *et al.* OpenSimRoot: widening the scope and application of root architectural models. *New Phytol* **215**, 1274-1286 (2017).
81 Watanabe, T. *et al.* Rice morphogenesis and plant architecture: Measurement, specification and the reconstruction of structural development by 3D architectural modelling. *Ann Bot* **95**, 1131-1143, doi:Doi 10.1093/Aob/Mci136 (2005).
82 Chang, T.-G. *et al.* A three-dimensional canopy photosynthesis model in rice with a complete description of the canopy architecture, leaf physiology, and mechanical properties. *J Exp Bot* **70**, 2479–2490, doi:10.1093/jxb/ery430 (2019).
83 Sonnewald, U. & Fernie, A. R. Next-generation strategies for understanding and influencing source–sink relations in crop plants. *Curr Opin Plant Biol* **43**, 63-70, doi:10.1016/j.pbi.2018.01.004 (2018).
84 Salon, C. *et al.* Fluxomics links cellular functional analyses to whole-plant phenotyping. *J Exp Bot* **68**, 2083-2098, doi:10.1093/jxb/erx126 (2017).
85 Cheung, F. Yield: The search for the rice of the future. *Nature* **514**, S60-S61 (2014).
86 Zhu, X. G., de Sturler, E. & Long, S. P. Optimizing the distribution of resources between enzymes of carbon metabolism can dramatically increase photosynthetic rate: A numerical simulation using an evolutionary algorithm. *Plant Physiol* **145**, 513-526, doi:DOI 10.1104/pp.107.103713 (2007).
87 Glass, A. D. M. *et al.* The regulation of nitrate and ammonium transport systems in plants. *J Exp Bot* **53**, 855-864, doi:DOI 10.1093/jexbot/53.370.855 (2002).
88 Pitman, M. & Cram, W. Regulation of inorganic ion transport in plants. *Ion Transport in Plants*, 465-481 (2013).
89 Henry, L. T. & Raper Jr, C. D. Soluble carbohydrate allocation to roots, photosynthetic rate of leaves, and nitrate assimilation as affected by nitrogen stress and irradiance. *Botanical Gazette*, 23-33 (1991).
90 Monod, J. The growth of bacterial cultures. *Annual Reviews in Microbiology* **3**, 371-394 (1949).
91 Miflin, B. & Lea, P. Ammonia assimilation. *The Biochemistry of Plants* **5**, 169-202 (1980).
92 Radin, J. W., Parker, L. L. & Sell, C. R. Partitioning of sugar between growth and nitrate reduction in cotton roots. *Plant Physiol* **62**, 550-553 (1978).
93 Muller, B. *et al.* Water deficits uncouple growth from photosynthesis, increase C content, and modify the relationships between C and growth in sink organs. *J Exp Bot*, erq438 (2011).
94 Willaume, M. & Pagès, L. Correlated responses of root growth and sugar concentrations to various defoliation treatments and rhythmic shoot growth in oak tree seedlings (*Quercus pubescens*). *Ann Bot*, mcq270 (2011).
95 Johnson, I. R. & Thornley, J. H. M. Dynamic model of the response of a vegetative grass crop to light, temperature and nitrogen. *Plant Cell Environ* **8**, 485-499, doi:10.1111/j.1365-3040.1985.tb01684.x (1985).
96 Asseng, S., Richter, C. & Wessolek, G. Modelling root growth of wheat as the linkage between crop and soil. *Plant Soil* **190**, 267-277, doi:10.1023/A:1004228201299 (1997).
97 Fanello, D. D., Bartoli, C. G. & Guiamet, J. J. Qualitative and quantitative modifications of root mitochondria during senescence of above-ground parts of *Arabidopis thaliana*. *Plant Sci* **258**, 112-121, doi:10.1016/j.plantsci.2017.01.013 (2017).
98 Von Caemmerer, S. *Biochemical models of leaf photosynthesis*. (Csiro publishing, 2000).
99 De Pury, D. & Farquhar, G. Simple scaling of photosynthesis from leaves to canopies without the errors of big-leaf models. *Plant, Cell & Environment* **20**, 537-557 (1997).
100 Tazoe, Y., Noguchi, K. & Terashima, I. Effects of growth light and nitrogen nutrition on the organization of the photosynthetic apparatus in leaves of a C_4 plant, Amaranthus cruentus. *Plant Cell Environ* **29**, 691-700 (2006).
101 San-oh, Y., Sugiyama, T., Yoshita, D., Ookawa, T. & Hirasawa, T. The effect of planting pattern on the rate of photosynthesis and related processes during ripening in rice plants. *Field Crops Res* **96**, 113-124 (2006).
102 Azcón-Bieto, J. Inhibition of photosynthesis by carbohydrates in wheat leaves. *Plant Physiol* **73**, 681-686 (1983).
103 Stitt, M. Rising CO_2 levels and their potential significance for carbon flow in photosynthetic cells. *Plant Cell Environ* **14**, 741-762 (1991).
104 Paul, M. J. & Pellny, T. K. Carbon metabolite feedback regulation of leaf photosynthesis and development. *Journal of experimental botany* **54**, 539-547, doi:10.1093/jxb/erg052 (2003).

105 Jarvis, P. The interpretation of the variations in leaf water potential and stomatal conductance found in canopies in the field. *Philosophical Transactions of the Royal Society of London B: Biological Sciences* **273**, 593-610 (1976).
106 Farquhar, G. D. & Sharkey, T. D. Stomatal conductance and photosynthesis. *Annu Rev Plant Physiol* **33**, 317-345 (1982).
107 Zhang, J. & Davies, W. Changes in the concentration of ABA in xylem sap as a function of changing soil water status can account for changes in leaf conductance and growth. *Plant Cell Environ* **13**, 277-285 (1990).
108 Leuning, R. A critical appraisal of a combined stomatal-photosynthesis model for C_3 plants. *Plant Cell Environ* **18**, 339-355 (1995).
109 Allen, R. G., Pereira, L. S., Raes, D. & Smith, M. Crop evapotranspiration-Guidelines for computing crop water requirements-FAO Irrigation and drainage paper 56. *FAO, Rome* **300**, D05109 (1998).
110 Andrews, M. The partitioning of nitrate assimilation between root and shoot of higher plants. *Plant Cell Environ* **9**, 511-519 (1986).
111 Nunes-Nesi, A., Fernie, A. R. & Stitt, M. Metabolic and signaling aspects underpinning the regulation of plant carbon nitrogen interactions. *Mol Plant* **3**, 973-996, doi:10.1093/mp/ssq049 (2010).
112 Walker, B. J., Strand, D. D., Kramer, D. M. & Cousins, A. B. The response of cyclic electron flow around photosystem I to changes in photorespiration and nitrate assimilation. *Plant Physiol* **165**, 453-462 (2014).
113 Pilkington, S. M. *et al.* Relationship between starch degradation and carbon demand for maintenance and growth in *Arabidopsis thaliana* in different irradiance and temperature regimes. *Plant Cell Environ* **38**, 157-171 (2015).
114 Feugier, F. G. & Satake, A. Dynamical feedback between circadian clock and sucrose availability explains adaptive response of starch metabolism to various photoperiods. *Front Plant Sci* **3**, 305 (2013).
115 Scialdone, A. *et al.* Arabidopsis plants perform arithmetic division to prevent starvation at night. *Elife* **2**, e00669 (2013).
116 Seaton, D. D., Ebenhöh, O., Millar, A. J. & Pokhilko, A. Regulatory principles and experimental approaches to the circadian control of starch turnover. *Journal of the Royal Society Interface* **11**, 20130979 (2014).
117 Yin, X. & van Laar, H. Crop Systems Dynamics: An Ecophysiological Model of Genotype-by-Environment Interactions (GECROS). *Wageningen Academic Pub., Wageningen* (2005).
118 Sinclair, T. & De Wit, C. Analysis of the carbon and nitrogen limitations to soybean yield. *Agron J* **68**, 319-324 (1976).
119 Masclaux‐Daubresse, C., Reisdorf‐Cren, M. & Orsel, M. Leaf nitrogen remobilisation for plant development and grain filling. *Plant Biol* **10**, 23-36 (2008).
120 Ou-Lee, T. M. & Setter, T. L. Enzyme activities of starch and sucrose pathways and growth of apical and basal maize kernels. *Plant Physiol* **79**, 848-851, doi:10.1104/pp.79.3.848 (1985).
121 Ober, E. S., Setter, T. L., Madison, J. T., Thompson, J. F. & Shapiro, P. S. Influence of water deficit on maize endosperm development : enzyme activities and RNA transcripts of starch and zein synthesis, abscisic acid, and cell division. *Plant Physiol* **97**, 154-164, doi:10.1104/pp.97.1.154 (1991).
122 Ohdan, T. *et al.* Expression profiling of genes involved in starch synthesis in sink and source organs of rice. *J Exp Bot* **56**, 3229-3244, doi:10.1093/jxb/eri292 (2005).
123 Toyosawa, Y. *et al.* Deficiency of starch synthase IIIa and IVb alters starch granule morphology from polyhedral to spherical in rice endosperm. *Plant Physiol* **170**, 1255-1270, doi:10.1104/pp.15.01232 (2016).
124 Cai, Y. *et al. OsPK2* encodes a plastidic pyruvate kinase involved in rice endosperm starch synthesis, compound granule formation and grain filling. *Plant Biotechnol J* **16**, 1878-1891, doi:10.1111/pbi.12923 (2018).
125 Olsen, O. A. Nuclear endosperm development in cereals and *Arabidopsis thaliana*. *Plant Cell* **16 Suppl**, S214-227, doi:10.1105/tpc.017111 (2004).
126 Yang, Z., Van Oosterom, E. J., Jordan, D. R. & Hammer, G. L. Pre-anthesis ovary development determines genotypic differences in potential kernel weight in sorghum. *J Exp Bot*, erp019 (2009).

127 Tashiro, T. & Wardlaw, I. F. A comparison of the effect of high temperature on grain development in wheat and rice. *Ann Bot* **64**, 59-65 (1989).
128 Lalonde, S., Tegeder, M., Throne‐Holst, M., Frommer, W. & Patrick, J. Phloem loading and unloading of sugars and amino acids. *Plant Cell Environ* **26**, 37-56 (2003).
129 Cannell, M. G. R. & Thornley, J. H. M. Modelling the components of plant respiration: Some guiding principles. *Ann Bot* **85**, 45-54, doi:DOI 10.1006/anbo.1999.0996 (2000).

Acknowledgements

This research was financially supported by the CAS (Chinese Academy of Science) strategic leading project (grant no. XDB27020105), the open research fund of the state key laboratory of hybrid rice (Hunan Hybrid Rice Research Center), and the national key research and development project (2018YFA0900600). The authors thank Prof. Govindjee for constructive comments and improving the language of the manuscript.

Author contributions

X.Z. designed the study; T.C. performed the analysis; T.C. and X.Z. wrote the manuscript.

Competing interests

The authors declare no competing financial interests

Supplementary Information

The following material is available in the online version of this article.

Supplementary Figure 1. Predicted relative changes of plant physiological traits for the wild type, the *ps1-D* mutant and the *OsNAP* RNAi plants.

Supplementary Figure 2. Predicted relative changes of plant physiological traits for the wild type, the *gif1* mutant and the *GIF1* overexpression plants.

Supplementary Figure 3. Predicted relative changes of plant physiological traits for 'source limited' plants with $v_{m_grain_Suc_ul}$ set to 100%, 50% and 200% of default values.

Supplementary Figure 4. The responses of major agronomic traits to the change in model parameters $v_{m_grain_Star_syn}$, $R_{_phloem_leaf_root}$, $v_{m_root_N_upt}$ and $v_{m_leaf_N_ass}$, respectively.

Supplementary Figure 5. The responses of major agronomic traits to the change in model parameters $v_{m_root_N_ass}$, $v_{m_leaf_Suc_l}$, $v_{m_leaf_IN_ul}$ and $v_{m_root_IN_l}$, respectively.

Supplementary Figure 6. The responses of major agronomic traits to the change in model parameters $v_{m_leaf_Star_deg}$, $v_{m_stem_Star_deg}$, $v_{m_leaf_Suc_syn}$ and $v_{m_leaf_Pro_deg}$, respectively.

Supplementary Figure 7. The responses of major agronomic traits to the change in model parameters $v_{m_leaf_ON_l}$, $v_{m_root_grow}$, $v_{m_leaf_Star_syn}$ and $v_{m_grain_Pro_syn}$, respectively.

Supplementary Figure 8. The responses of major agronomic traits to the change in

model parameters $v_{m_grain_ON_ul}$, $v_{m_grain_grow}$, $v_{m_grain_Suc_ul}$ and $R_{_phloem_leaf_grain}$, respectively.

Supplementary Figure 9. The responses of major agronomic traits to the change in model parameters $v_{m_root_Suc_ul}$, $v_{m_root_ON_l}$, $v_{m_ON_Vbtransfer}$ and $v_{m_stem_Star_syn}$, respectively.

Supplementary Figure 10. The responses of major agronomic traits to the change in model parameters $v_{m_leaf_Pro_syn}$, $v_{m_stem_Pro_deg}$, $v_{m_root_ON_ul}$ and $v_{m_stem_Pro_syn}$, respectively.

Supplementary Figure 11. The evolution of total grain yield throughout generations in the *in silico* 'evolutionary populations'.

Supplementary Figure 12. Distribution of relative values of plant initial size related parameters at the flowering stage for *in silico* high-yield 'Elite' individuals.

Supplementary Figure 13. WACNI predictions of grain filling patterns for plants in *in silico* evolutionary populations.

Supplementary Figure 14. Daily weather data of the normal condition used in WACNI.

Supplementary Table 1. Detailed description and comprehensive parameterization procedure of the parameters used in WACNI.

Supplementary Table 2. Effects on eight agronomic traits, obtained by manipulating candidate genes and/or QTLs responsible for capacities of 28 reaction and diffusion processes in WACNI.

Supplementary Table 3. Functional description of genes in Table S2.

Supplementary Datasets 1. 'Supplementary Datasets 1 paras_of_elites.xlsx'. Parameter values (relative fold change from default values) of 'Elite' individuals and the final grain weight and grain nitrogen concentration.

Supplementary Datasets 2. 'Supplementary Datasets 2 experimental_data_from_literature.xlsx'. Details of experimental data extracted from literature that used in model parameterization and model-data comparison (Figures 2-4).